The linear stability of dilute particulate rings

Henrik N. Latter [a,*], Gordon I. Ogilvie [a]

[a] *DAMTP, University of Cambridge, CMS, Wilberforce Road, Cambridge CB3 0WA, UK*

Abstract

Irregular structure in planetary rings is often attributed to the intrinsic instabilities of a homogeneous state undergoing Keplerian shear. Previously these have been analysed with simple hydrodynamic models. We instead employ a kinetic theory, in which we solve the linearised moment equations derived in Shu and Stewart 1985 for a dilute ring. This facilitates an examination of velocity anisotropy and non-Newtonian stress, and their effects on the viscous and viscous/gravitational instabilities thought to occur in Saturn's rings. Because we adopt a dilute gas model, the applicability of our results to the actual dense rings of Saturn are significantly curtailled. Nevertheless this study is a necessary preliminary before an attack on the difficult problem of dense ring dynamics.

We find the Shu and Stewart formalism admits analytic stability criteria for the viscous overstability, viscous instability, and thermal instability. These criteria are compared with those of a hydrodynamic model incorporating the effective viscosity and cooling function computed from the kinetic steady state. We find the two agree in the 'hydrodynamic limit' (i.e. many collisions per orbit) but disagree when collisions are less frequent, when we expect the viscous stress to be increasingly non-Newtonian and the velocity distribution increasingly anisotropic. In particular, hydrodynamics predicts viscous overstability for a larger portion of parameter space. We also numerically solve the linearised equations of the more accurate Goldreich and Tremaine 1978 kinetic model and discover its linear stability to be qualitatively the same as that of Shu and Stewart's. Thus the simple collision operator adopted in the latter would appear to be an adequate approximation for dilute rings, at least in the linear regime.

Key words: Planetary Rings, Collisional Physics

* Corresponding author.
Email addresses: hl278@cam.ac.uk (Henrik N. Latter), gio10@cam.ac.uk (Gordon I. Ogilvie).

1 Introduction

This paper examines the collisional dynamics of differentially rotating, particulate disks, and addresses specifically the intrinsic mechanisms which might induce the generation of irregular, fine-scale structure, such as that exhibited by Saturn's B-ring. *Voyager*, and *Cassini* more recently, revealed that these essentially axisymmetric variations appear on a very wide range of length-scale– from the limit of resolution ($\sim$ 100m) to several hundred kilometres (Horn and Cuzzi 1995, Porco *et al.* 2005). Though some proportion of B-ring structure may be caused by non-dynamical effects such as variations in albedo and phase function- see Cuzzi and Estrada 1996, for example) and from gravitational interactions with neighbouring satellites (Thiessenhusen *et al.* 1995), it is believed that the majority corresponds to changes in optical thickness resulting from a collective dynamics (Tremaine 2003).

This work studies *dilute* particulate systems, and as such may not be directly applicable to the saturnian rings. It is nevertheless an informative first stop before we embark on the challenging stability analysis of a dense granular gas. Other than presenting a general framework in which such a calculation can be tackled, the dilute gas formalism permits us to isolate analytically the interesting effects of anisotropy and non-Newtonian viscous stress upon the local axisymmetric instabilities thought to be manifest in planetary rings.

Since *Voyager* first reported the radial stratification of Saturn's rings, theoreticians have advocated a number of possible causes. These have included: ballistic transport (Durisen 1995), electromagnetic effects (Goertz and Morfill 1988), and interleaved shearing and shear-free zones (Tremaine 2003). Others have looked to the local instabilities of viscous fluid disks, interpreting the disordered state observed as the saturated endpoint of their nonlinear evolution. The 'viscous instability' was the first proposed (Lin and Bodenheimer 1981, Ward 1981, and Lukkari 1981). Essentially a monotonic 'clumping', it is associated with an outward angular momentum flux which decreases with surface density: $d(\nu\sigma)/d\sigma < 0$ (where ν is kinematic viscosity and σ surface mass density). Though a dilute ring's viscosity depends on optical depth in a manner which promises the existence of such an instability (Goldreich and Tremaine 1978, Shu and Stewart 1985), Saturn's rings are most likely 'dense', and theoretical and numerical N-body studies have revealed that such rings do not manifest the appropriate viscosity for this instability to develop (Araki and Tremaine 1986, and Wisdom and Tremaine 1988).

The 'viscous overstability' was first examined in the context of accretion disks by Kato (1978), and, as the name suggests, originates in overcompensation by the system's restoring forces: the stress oscillation which accompanies the epicyclic response in an acoustic-inertial wave will force the system back to

equilibrium so strongly that it will 'overshoot'. The mechanism relies on: a) the synchronisation of the viscous stress's oscillations with those of density, and b) the viscous stress increasing sufficiently in the compressed phase. In hydrodynamics only the latter consideration is relevant, which furnishes the criterion for overstability: $\beta \equiv (d\ln\nu/d\ln\sigma) > \beta^*$, where β^* is a number dependent on the thermal properties of the ring (Schmit and Tscharnuter 1995).

The viscous overstability has been a favoured explanation for smaller scale B-ring structure in recent years, a status stemming, primarily, from the viscosity profiles computed by Araki and Tremaine's 1986 dense gas model and Wisdom and Tremaine's 1988 particle simulations. Both appear to satisfy the above criterion. Consequently the linear behaviour of the instability has been thoroughly examined, though only within a hydrodynamic framework (Schmit and Tscharnuter 1995, Spahn *et. al.* 2000, and Schmidt *et al.* 2001). In addition, Schmidt and Salo (2003) have constructed a weakly nonlinear theory, and the overstability's long-term, nonlinear behaviour has been numerically studied by Schmit and Tscharnuter (1999). An isothermal model was adopted in both cases.

However, fluid mechanics is only one of several theoretical approaches thathave been deployed to capture the behaviour of planetary rings: N-body simulations, generalisations of stellar dynamics, and kinetic theory. This plurality is surely indicative of how the field of planetary ring dynamics falls uncomfortably between the more familiar frameworks of classical physics. Our analysis will predominantly focus upon the kinetic approach, and solve the set of moment equations derived from the kinetic theories proposed in Shu and Stewart 1985 (hereafter referred to as 'SS85') and in Goldreich and Tremaine 1978 (referred to as 'GT78'). These formalisms have hitherto been used mainly to establish equilibrium solutions. This paper goes the next step by exploring their linear theory.

Such an analysis is more involved than the analogous hydrodynamic calculation; however, the latter's adoption of the Navier-Stokes stress model introduces two assumptions which may be inappropriate in the ring context and whose consequences are instructive to investigate. Firstly, the Navier-Stokes model presumes the distribution of the particles' velocity dispersion to be nearly isotropic. In the regime of many collisions per orbit this is an acceptable supposition, as collisions scatter particles randomly on the average. However if the collision rate, ω_c, is of the same order as the orbital frequency, Ω, (as it is presumed to be in Saturn's rings) this need not be true. Secondly, hydrodynamics assumes an 'instantaneous' (local in time) relationship between stress and strain. This may not hold when $\omega_c \sim \Omega$. Generally the viscous stress possesses a relaxation time of order $1/\omega_c$, which in this regime will be comparable

to the dynamic time scale. Thus the immediate history of the stress cannot be ignored. Its inclusion should have the most impact on the stability of oscillating modes, especially the overstability, it depending on the synchronisation of the stress and density oscillations. A kinetic model can address both issues, accounting for anisotropy within an appropriate collision term and providing a straightforward way, by the taking of moments, to generate dynamical equations for the viscous stress. Another advantage is that a kinetic model lets us explicitly include the microphysics of particle-particle interactions and thence to potentially model a larger set of the physical mechanisms at play (such as collisions, irregular surfaces, spin , size distribution, etc). It also narrows the scope of our simplifying assumptions to the particulars of collisions between spheres of ice, which have been observed in the laboratory (see Bridges *et al.* 1984, Hatzes *et al.* 1988, amongst others) .

The paper is organised as follows. In Section 2 we present a brief derivation of the set of closed, vertically averaged moment equations in a local model, the shearing sheet, for a general kinetic equation. We then specialise to the SS85 kinetic model and briefly exhibit its equilibrium characteristics. Section 3 contains the linear theory of a general kinetic equation and proves results pertaining to self-gravity and the thermal modes when in the limit of length-scales much longer than the disk height. We then derive stability criteria for the viscous instability and overstability specific to the SS85 model. Comparisons with an analogous calculation for a hydrodynamic model and the GT78 model are performed in Sections 4 and 5. In the former we isolate the effects of non-Newtonian stress on the linear theory, and in the latter observe how the SS85 collision term approximates satisfactorily that of the more accurate triaxial Gaussian model. We draw our conclusions in Section 6.

2 Kinetic Model

2.1 Simplifying Assumptions

The formulation of a suitable kinetic theory poses a number of difficulties, namely the closure of the moment hierarchy and the simplification of the collision term. But the various approximations these require by no means cripple the approach. The most fundamental assumption we make is that our ring is composed exclusively of hard, identical, and indestructible spheres. In addition we presume that the particles are non-spinning. These simplifications render the mathematics convenient (but see Stewart *et al.* 1984 and Shu and Stewart 1985 for justifications)– now the inelasticity of the collisions is quantified solely by the normal coefficient of restitution, ε, which is the ratio of the

normal relative speed after and before a collision. It is generally a function of normal impact velocity, v_n, and possibly other parameters like ambient temperature and pressure, particle size and mass (Hatzes *et al.* 1988, Dilley 1993) .

A number of laboratory experiments have been conducted in order to ascertain the collisional properties of ice spheres in saturnian conditions, in particular the relationship between the coefficient of restitution and v_n (see Bridges *et al.* 1984, Hatzes *et al.* 1988, Supulver *et al.* 1995, and Dilley and Crawford 1996). Excepting Dilley, these authors successfully fit a step-wise power law to their data for collisions sufficiently gentle and/or surfaces sufficiently frosted:

$$\varepsilon(v_n) = \begin{cases} (v_n/v_c)^{-p}, & \text{for} \quad v_n > v_c, \\ 1, & \text{for} \quad v_n \leq v_c, \end{cases} \tag{1}$$

where v_c and p are parameters contingent on the material properties of the ice balls and their ambient environment. Bridges' data admit $p = 0.234$ and $v_c = 0.0077$ cm s^{-1} for frosted particles of radius 2.5cm at a temperature of 210K (significantly higher than the appropriate conditions). Hatzes finds $p = 0.20$ and $v_c = 0.025$ cm s^{-1} for the case of frosted particles at 123K (however, for the case of smoother particles an exponential law provides a better fit). At slightly lower temperatures ($\approx$100K) Supulver *et al.* obtain $p = 0.19$ and $v_c = 0.029$ cm s^{-1} with their torsional pendulum fixed. Though the functional relationship (1) is useful, the coefficient of restitution varies considerably as the physical condition of the contact surface is more or less frosty or sublimated, as Hatzes *et al.* explore. Also the neglect of spin, the effects of glancing collisions, irregularly shaped surfaces, coagulation and erosion, mass transfer and the role of amorphous ice, further emphasises the simplicity of the collision model adopted. Studies of those processes we omit are found in Salo 1987, Araki 1991 and Morishima and Salo 2006 (theory and simulations), and in McDonald *et al.* 1989, Hatzes *et al.* 1991, Supulver *et al.* 1995 and Supulver *et al.* 1997 (experiments).

From this point on we denote by ε the *averaged* coefficient of restitution, which is a function of the macroscopic variable, c, the velocity dispersion. For a general step-wise power law and a Maxwellian velocity distribution, it is straightforward to obtain an analytic expression for ε averaged over collisions. Its functional dependence on c is, unsurprisingly, the 'smoothed' analogue of Eq.(1)'s piecewise dependence on v_n.

The rings we study are *dilute*. We realise this curtails the applicability of our results considerably as Saturn's rings, even the optically thin regions, are thought to exhibit important dense effects. Araki and Tremaine (1986) revealed significant collisional contributions to the kinetic equilibrium when collisions are sufficiently inelastic; and the experimentally derived elasticity

laws of (1) predict collisions are dissipative enough for this 'cold' regime to be widespread in Saturn's rings, given appropriate particle sizes (see Marouf *et al.* 1983 and Zebker *et al* 1985). This conclusion has been confirmed by particle simulations, Wisdom and Tremaine 1988 and Salo 1991 the most notable. Moreover, both simulations and theoretical models show that the dynamics of small particles (for which nonlocal effects are less important) strongly couple to the dynamics of the largest particles (for which nonlocal effects *are* important), both in two size systems and in polydisperse disks exhibiting power-law size distributions akin to Saturn's (see Stewart *et al.* 1984, Salo 1987, Lukkari 1989, Salo 1991, and Salo 1992b).

Physically then, a dilute model best describes planetary rings in which the radii of the largest particles are of the order of centimetres, or tens of centimetres. Estimates on the maximum size of particle radius are easy to establish from the dilute theory, though these are only *necessary* bounds: sufficient conditions for the applicability of the dilute model can only be determined from the dense theory. At lower optical depths, however, we expect the dilute estimates to serve as a reasonable guide. We obtain these by combining the famous equilibrium relation between optical thickness, τ, and ε, computed in GT78 (cf. Fig 7), with the elasticity laws embodied in (1). This determines the dependence of velocity dispersion on τ. We then suppose that non-local effects may be neglected if a particle's r.m.s. speed, $\sqrt{3}c$, is an order larger than the shear velocity across two particle radii, $3\Omega a$, where a is particle radius (Araki 1991)– the ratio of these quantities is a convenient measure of 'nonlocality', but only for optical thicknesses less than about 1 or 2 (see Salo 1991). Thereupon we compute an upper limit on a below which the dilute model is acceptable. If $\tau = 0.2$ at C-ring distances, $a_{\max}$ ranges from 31cm (for Supulver *et al.*'s data) to 5.3cm (for Bridges *et al.*'s data). At A-ring distances for $\tau = 0.5$ the maximum particle radius is 33cm (Supulver *et al.*) or 6.3cm (Bridges *et al.*). At B-ring distances and $\tau = 1$, the Bridges *et al.* data imply $a_{\max} \approx 2.2$cm, or, alternatively, $v_c \approx 0.35$ cm s^{-1} for metre-sized particles. This last estimate appears consistent with those simulations of Salo (1991) in which v_c was increased to 20 and 40 times $v_B = 0.01$ cm/s (cf. his Fig.'s 5a, 5c and 5d). It is interesting to note the sensitivity of the critical a to the elasticity law adopted: relations which predict slightly less dissipative impacts allow a substantially higher velocity dispersion, and subsequently $a_{\max}$.

Our dilute ring is self-gravitating. Disk self-gravity may be decomposed into three effects. Firstly, inter-particle gravitational forces will lead to an additional source of (elastic) scattering via gravitational encounters. They will also enhance the collision frequency of physical collisions (gravitational focusing). For either process to be appreciable, the velocity dispersion must be of order the particles' escape velocity, i.e. $G\rho a^2 \sim c^2$, where G is the gravitation constant and ρ the mass density of the particle material. This can be recast

as $(a\Omega)/c \sim 1$, for typical values of the saturnian system. As non-local effects are neglected, the left side of this scaling will be $\ll 1$, and hence gravitational scattering and focusing may be omitted. Secondly, the aggregate of all the particle attractions will increase the disk's vertical restoring force and further flatten the disk. Subsequently the collision frequency will increase, an effect which we include. Thirdly, there will arise a dynamical contribution to the disk's stability which issues from the extra term in the momentum equation. Though this term will be unimportant at equilibrium, being dominated by the planet's gravitational potential, it will be significant in the linear theory. As is well known, an inviscid fluid disk collapses under the action of self-gravity for a Toomre parameter Q less than 1, its unstable modes growing on a band of intermediate wavelengths, with rotation and pressure stabilising the long and short scales respectively (Toomre 1964, Julian and Toomre 1966). A viscous disk however paints a slightly more complex picture. Then it is better to think of self-gravity as 'extending' the viscous instabilities we discuss into larger areas of parameter space. In these 'extensions' the instabilities grow only in a certain confined range of intermediate wavelength, unlike the non-self-gravitating case in which the longest wavelengths are the first to become viscously unstable and overstable (Schmit and Tscharnuter 1995). We shall examine this effect in some detail particularly for the viscous instability. We should mention also that self gravity induces transient, non-axisymmetric wakes, the analysis of which we omit (but see Salo 1992a).

2.2 The Governing Moment Equations

Consider a dilute gas of identical, smooth, inelastic spheres of mass m with phase space distribution $f(\mathbf{x}, \mathbf{v}, t)$. The number of particles located in the volume $d\mathbf{x}$ centred at $\mathbf{x}$ with velocities in the range $d\mathbf{v}$ centred at $\mathbf{v}$ at time t is defined as $f(\mathbf{x}, \mathbf{v}, t) d\mathbf{x}\, d\mathbf{v}$. Taking moments of f allows us to calculate the familiar macroscopic characteristics of the gas. Number density, n, bulk velocity, $\mathbf{u}$, and velocity dispersion, c, are defined through

$$n(\mathbf{x}, t) \equiv \int f \, d\mathbf{v}, \tag{2}$$

$$n\mathbf{u}(\mathbf{x}, t) \equiv \int \mathbf{v} f \, d\mathbf{v}, \tag{3}$$

$$\frac{3}{2} n c^2(\mathbf{x}, t) \equiv \int \frac{1}{2} |\mathbf{v} - \mathbf{u}|^2 \, f d\mathbf{v}. \tag{4}$$

The phase space distribution satisfies a kinetic equation which is distinguished by a collision operator, $(\partial f/\partial t)_c$, whose precise form reflects the collisional microphysics.

We situate our gas in a *shearing sheet*. This is a convenient representation of a differentially rotating disk in which a small patch, centred on a point moving

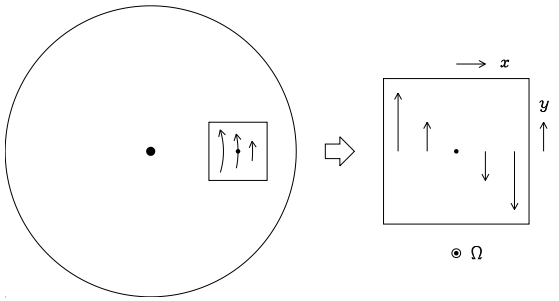

Fig. 1. The shearing sheet. The differential rotation is locally represented as a rotation superimposed upon a linear shear flow.

on a circular orbit at $r = r_0$, is represented as a sheet in uniform rotation, $\Omega(r_0)\,\mathbf{e}_z$, and subjected to a linear shear flow, $\mathbf{u}_0 = -2A_0 x\,\mathbf{e}_y$. The local rectilinear coordinates x and y point in the radial and azimuthal directions respectively, and $A_0 = -\frac{1}{2} r_0 (d\Omega/dr)_0$; see Fig. 1. For the dynamical analysis we consider the sheet horizontally unbounded, at least compared to the vertical length scale of the disk. The model hence provides an excellent approximation for rings whose thickness is very small, such as Saturn's.

In terms of the peculiar velocity, $\mathbf{w} = \mathbf{v} - \mathbf{u}$, the kinetic equation for such a patch of ring is

$$\frac{\partial f}{\partial t} + (w_i + u_i)\frac{\partial f}{\partial x_i} - \left[\frac{\partial u_i}{\partial t} + (w_j + u_j)\frac{\partial u_i}{\partial x_j} - F_i\right]\frac{\partial f}{\partial w_i} = \left(\frac{\partial f}{\partial t}\right)_c, \qquad (5)$$

where the force/unit mass is

$$F_i = -\frac{\partial(\phi_P + \phi_D)}{\partial x_i} - 2\epsilon_{ijk}\Omega_j(w_k + u_k).$$

The appropriate centrifugal-gravitational potential of the planet is denoted by ϕ_P, and the disk's gravitational potential by ϕ_D. The tensor ϵ_{ijk} is the alternating tensor and the angular velocity is $\mathbf{\Omega} = \Omega_0\,\mathbf{e}_z$, where $\Omega_0 = \Omega(r_0)$. By multiplying (5) by 1, w_i and $w_i w_j$ and then integrating over all $\mathbf{w}$ we derive the continuity equation,

$$\partial_t n + \partial_k(n u_k) = 0, \qquad (6)$$

the equation of motion,

$$n\,(\partial_t u_i + u_k \partial_k u_i) = -2n\epsilon_{ijk}\Omega_j u_k - n\partial_i(\phi_P + \phi_D) - \partial_j p_{ij}, \qquad (7)$$

and the pressure tensor equation,

$$\partial_t p_{ij} + u_k \partial_k p_{ij} = -p_{ik}\partial_k u_j - p_{jk}\partial_k u_i - p_{ij}\partial_k u_k - 2\epsilon_{ikl}\Omega_k p_{lj} - 2\epsilon_{jkl}\Omega_k p_{li} - \partial_k p_{ijk} + q_{ij}, \qquad (8)$$

where p_{ij} and p_{ijk} are the second and third-order moments,

$$p_{ij\ldots} = \int w_i w_j \ldots f d\mathbf{w},$$

and the collisional change in second moment is

$$q_{ij} = \int w_i w_j \left(\frac{\partial f}{\partial t}\right)_c d\mathbf{w},$$

which is a yet to be specified function of the other field variables. For notational brevity we have set $\partial_i = \partial/\partial x_i$.

As we are interested in scales $\gg H$ there is little point in solving for a disk's detailed vertical structure. We hence vertically integrate the moment equations, a process which can be performed without much grief if it is assumed that u_x and u_y are effectively independent of z. The third order moments are neglected. This move closes the system but restricts the applicability of the equations to behaviour on lengthscales much larger than the disk thickness. If the system exhibits variation on scales close to H the vertically integrated equations will most likely predict incorrect behaviour.

We now have:

$$D_t N = -N\partial_\alpha u_\alpha, \tag{9}$$

$$N D_t u_\alpha = -N\partial_\alpha(\Phi_P + \Phi_D) - 2N\epsilon_{\alpha z\gamma}\Omega_0 u_\gamma - \partial_\beta P_{\alpha\beta}, \tag{10}$$

$$D_t P_{ij} = -P_{ij}\partial_\gamma u_\gamma - P_{j\gamma}\partial_\gamma u_i - P_{i\gamma}\partial_\gamma u_j - 2\epsilon_{izk}\Omega_0 P_{kj} - 2\epsilon_{jzk}\Omega_0 P_{ki} + Q_{ij}, \tag{11}$$

where $D_t = \partial_t + u_\gamma\partial_\gamma$, Greek indices run only from x to y and upper case denotes vertical integration. Optical thickness is subsequently defined as $\tau = \pi a^2 N$. To complete the set, expressions for Φ_P and Φ_D are required. We approximate the central body as perfectly spherical, which accounts for the former potential; the latter must be obtained from Poisson's equation:

$$\nabla^2\phi_D = 4\pi m G n, \tag{12}$$

in which we may approximate n by $N\delta(z)$, if it is assumed the disk is very thin. An additional equation for the mean vertical displacement of the disk, Z, can be supplied from the z component of the equation of motion (see SS85), and the instances of u_z in (11) are identified with its rate of change, $D_t Z$. But we shall not be investigating the vertical warping of the disk and shall assume symmetry about the plane $z = 0$. Hence $Z = P_{xz} = P_{yz} = 0$.

It is often illuminating to work with the internal energy and viscous stress equations in place of (11). The former equation may be procured by taking half

the trace of (11) and defining $3NC^2 \equiv P_{ii}$, where C is the vertically averaged velocity dispersion. A viscous stress equation proceeds by subtracting (11) from $2\delta_{ij}/3$ times the energy equation, if we define the viscous stress tensor as

$$\Pi_{ij} \equiv NC^2\delta_{ij} - P_{ij}.$$

We omit these details (see SS85).

2.3 The SS85 Model

We specialise to the modified BGK collision term (Bhatnagar *et al.* 1954) which Shu and Stewart introduce in SS85:

$$\left(\frac{\partial f}{\partial t}\right)_c = \omega_c(f_I - f).$$

Here ω_c designates the collision frequency and f_I is the equilibrium distribution function to which the collisional process tends to push the system. This is set equal to a Maxwellian. Essentially the model ensures that all particles which undergo a collision at a certain time will be distributed immediately afterwards like f_I. Given that on the average collisions randomize velocity dispersion, this is not a bad approximation, but it does downplay the particles' distribution immediately prior to the collision: if f is very far from a Maxwellian, the BGK model could overestimate the isotropizing power of collisions.

In order to account for the inelasticity of the particle collisions Shu and Stewart attribute to f_I the same n and $\mathbf{u}$ as f (in order to conserve mass and momentum), but set its velocity dispersion c_I^2 less than c^2. They then assume energy equipartition which permits them to write

$$c_I^2 = (2 + \varepsilon^2)c^2/3, \tag{13}$$

where the coefficient of restitution ε is here understood to be a quantity averaged over collisions. The approximation of energy equipartition will worsen the further f departs from Maxwellian, and may explain the discrepancy between the results of SS85 and GT78 in the collisionless limit.

To complete the model Shu and Stewart present an expression for the vertically averaged collision frequency. They find that, for a dilute, vertically isothermal disk with a locally Maxwellian velocity distribution,

$$\omega_c = 8\Omega_z a^2 N \quad (= 8\Omega_z \tau/\pi) \tag{14}$$

where Ω_z is the vertical epicyclic frequency. In this case the collision frequency depends solely and linearly on N, and not on C. As it stands this expressions

fails to capture the influence of anisotropy. But it can be improved on this count, somewhat, via inclusion of a factor $\sqrt{NC^2/P_{zz}}$, which comes from modifying the scale height of the disk from c/Ω_z to c_z/Ω_z, where c_z is the vertical velocity dispersion.

The influence of self-gravity on the vertical epicyclic oscillation may be approximated through

$$\Omega_z^2 = \Omega_0^2 + (\partial_z^2 \phi_D)_{z=0}.$$

If we assume ϕ_D varies slowly with x and y, then $\nabla^2 \approx \partial_z^2$ in Poisson's equation, and with $n \propto \exp(-z^2/(2H^2))$ this renders ω_c's dependence on surface number density like:

$$\omega_c \approx 8a^2\,\Omega_0\,N\sqrt{1 + (2\sqrt{2\pi}Gm/H\Omega_0^2)\,N}. \tag{15}$$

Hence ω_c can vary as steeply as $N^{3/2}$ in a self-gravitating disk, and at equilibrium self-gravity enhances the collision frequency by a factor $\sqrt{1 + 2\sqrt{2/\pi}\,Q^{-1}}$, where Q is the Toomre parameter.

2.4 The Shu & Stewart Equilibrium Disk

The equilibrium homogeneous state of Keplerian shear can be computed analytically if the SS85 term is included, for which

$$Q_{ij} = \omega_c(N\,C_I^2\delta_{ij} - P_{ij}).$$

Let $\omega_c = \omega_c(N)$. Then, given a uniform density N_0 and shear rate $\mathbf{u}_0 = -\frac{3}{2}\Omega_0\,x\,\mathbf{e}_y$, the uniform viscous stress tensor and the equilibrium value of ε proceed from (11). The averaged coefficent of restitution ε depends on C uniquely and, once its equilibrium value is set, C_0 can be deduced from the average of Eq.(1). The solution is

$$\mathbf{\Pi}_0 = \frac{3N_0C_0^2}{11 + 2(\omega_0/\Omega_0)^2}\begin{pmatrix} -3 & -\omega_0/\Omega_0 & 0 \\ -\omega_0/\Omega_0 & 2 & 0 \\ 0 & 0 & 1 \end{pmatrix} \tag{16}$$

and

$$\varepsilon_0 = \sqrt{1 - \frac{9}{11 + 2(\omega_0/\Omega_0)^2}}, \tag{17}$$

for $\omega_0 \equiv \omega_c(N_0)$ and $\varepsilon_0 \equiv \varepsilon(C_0^2)$.

The form of Π_{xy} demonstrates a local relationship between shear and stress.

Therefore one may write down the effective kinematic viscosity,

$$\nu = \left(\frac{C_0^2}{\Omega_0}\right) \frac{2(\omega_0/\Omega_0)}{11 + 2(\omega_0/\Omega_0)^2}, \tag{18}$$

as a function of ω_0. Note the implicit dependence on ω_0 through C_0: the equilibrium velocity dispersion depends on ε_0 which in turn is set by ω_0. In the hydrodynamic limit, $\omega_0/\Omega_0 \to \infty$, the viscosity must keep momentum flux constant and thus goes to zero like $(\omega_0/\Omega_0)^{-1}$ (Chapman and Cowling 1970). But in the collisionless limit the viscosity approaches 0 like ω_0/Ω. In this regime the trajectories of particles between collisions are long and subject to epicyclic confinement. As a consequence angular momentum transport is inefficient. Because the effective viscosity vanishes in both limits there exists a turning point in the intermediate range when the gas is hot yet not too rarefied. A simple calculation shows that this turning point occurs at $\omega_0 = \widetilde{\omega}$, where

$$\widetilde{\omega} = \tfrac{1}{2}\,\Omega_0 \sqrt{9(1 + 2/e) + \sqrt{81(1 + 2/e)^2 + 88}}, \tag{19}$$

the definition of which introduces the important parameter

$$e \equiv (d \ln \varepsilon^2 / d \ln C^2)_0. \tag{20}$$

For a piecewise power-law, this parameter depends on both p and C_0/v_c, but only weakly for the latter: we can roughly approximate e with $-p$. Hydrodynamics would suggest that one look to the region $\omega_0 > \widetilde{\omega}$ to observe viscous instability and to $\omega_0 < \widetilde{\omega}$ for viscous overstability. Because the system is dilute and the particles non-spinning there is no effective bulk viscosity.

As Goldreich and Tremaine argue, energetic instability is assured if $e \geq 0$. Consider a small deviation in C^2 *below* its equilibrium value. When $e > 0$ this change will generate a small decrease in ε and a converse increase in collisional dissipation per collision (on the average). Thence cooling will slightly dominate viscous heating and thus amplify the disturbance, initiating a runaway loss of energy. A small deviation *above* equilibrium on the other hand causes a decrease in collisional cooling, which will precipitate a runaway heating. If $e = 0$ the velocity dispersion cannot adjust either way to balance the energy budget, and so the system will also be unstable. For $e < 0$ the velocity dispersion will act to return the system to equilibrium if thermally disturbed, and the speed of return is proportional to the magnitude of e. Isothermality in our model hence corresponds to $e \to -\infty$, as then any thermal perturbation will be 'instantly' quenched. Of course 'instant quenching' is an artefact of the averaging process; in reality a particulate disk may return to thermal equilibrium no faster than the collision time, nor could an averaged ε exhibit a steep enough dependence on c to yield e very large and negative.

A more general perturbation including density displacements complicates the

simple heuristic picture sketched above, but on long lengthscales the above argument should hold.

3 Linear Stability Calculation

3.1 General Results

In this section we establish the linear stability of the moment equations. We begin by presenting a number of results which hold for a second-order system derived from a kinetic equation with an unspecified collision term.

Consider the vertically integrated equations:

$$D_t N = -N\partial_\alpha u_\alpha, \tag{21}$$

$$D_t u_\alpha = -\partial_\alpha(\Phi_P + \Phi_D) - 2\epsilon_{\alpha z\beta}\Omega_0 u_\beta - \frac{1}{N}\partial_\beta P_{\alpha\beta}, \tag{22}$$

$$D_t P_{ij} = -P_{i\gamma}\partial_\gamma u_j - P_{j\gamma}\partial_\gamma u_i - P_{ij}\partial_\gamma u_\gamma - 2\Omega_0(\epsilon_{izk}P_{kj} + \epsilon_{jzk}P_{ki}) + Q_{ij}, \tag{23}$$

in a shearing sheet for a general collision term, $Q_{ij} = Q_{ij}(N, \mathbf{P})$.

Now suppose Eq.'s (21)–(23) admit a homogeneous steady state characterised by the equilibrium number density N_0, Keplerian shear $\mathbf{u}_0 = (0, -3\Omega_0\, x/2)$ and equilibrium pressure tensor $\mathbf{P}^0$. Let us perturb this solution with a small axisymmetric disturbance:

$$\begin{aligned} N &= N_0 + \hat{N}(x,t), \\ \mathbf{u} &= -(3\Omega_0\, x/2)\mathbf{e}_y + \{u(x,t)\mathbf{e}_x + v(x,t)\mathbf{e}_y\}, \\ \mathbf{P} &= \mathbf{P}^0 + \hat{\mathbf{P}}(x,t), \end{aligned}$$

for $|\hat{N}| \ll N_0$, $|\nabla(u,v)| \ll \Omega_0$ and $|\hat{\mathbf{P}}| \ll |\mathbf{P}^0|$, then take the solution of the linearized Poisson equation to be

$$\hat{\Phi}_D = -\frac{2\pi G m}{|k|}\hat{N},$$

in which k is the wavenumber of the harmonic variation of $\hat{N}$ (Binney and Tremaine 1987).

Next we nondimensionalise: time according to the orbital timescale, $t = t^*/\Omega_0$; space like $\mathbf{x} = (C_0/\Omega_0)\mathbf{x}^*$; surface density by N_0; velocity by C_0 and the

pressure tensor by $N_0 C_0^2$. On dropping the stars and linearising we acquire

$$\begin{aligned}
\partial_t \hat{N} &= -\partial_x u, \\
\partial_t u &= (2g/|k|)\partial_x \hat{N} + 2v - \partial_x \hat{P}_{xx}, \\
\partial_t v &= -\tfrac{1}{2}u - \partial_x \hat{P}_{xy}, \\
\partial_t \hat{P}_{xx} &= -3P^0_{xx}\partial_x u + 4\hat{P}_{xy} + \hat{Q}_{xx}, \\
\partial_t \hat{P}_{xy} &= -2P^0_{xy}\partial_x u - P^0_{xx}\partial_x v - \tfrac{1}{2}\hat{P}_{xx} + 2\hat{P}_{yy} + \hat{Q}_{xy} \\
\partial_t \hat{P}_{yy} &= -P^0_{yy}\partial_x u - 2P^0_{xy}\partial_x v - \hat{P}_{xy} + \hat{Q}_{yy}, \\
\partial_t \hat{P}_{zz} &= -P^0_{zz}\partial_x u + \hat{Q}_{zz}.
\end{aligned}$$

The perturbed collision terms take the form

$$\hat{Q}_{ij} = \left(\frac{\partial Q_{ij}}{\partial N}\right)_0 \hat{N} + \left(\frac{\partial Q_{ij}}{\partial P_{xx}}\right)_0 \hat{P}_{xx} + \left(\frac{\partial Q_{ij}}{\partial P_{xy}}\right)_0 \hat{P}_{xy} + \left(\frac{\partial Q_{ij}}{\partial P_{yy}}\right)_0 \hat{P}_{yy} + \left(\frac{\partial Q_{ij}}{\partial P_{zz}}\right)_0 \hat{P}_{zz},$$

and self-gravity is expressed in the parameter g defined by

$$g = \frac{\pi G N_0 m}{C_0 \Omega_0}, \tag{24}$$

which is the inverse of the Toomre Q parameter.

We perform a Fourier decomposition into radial modes for each perturbed quantity so that they are $\propto \exp(ikx + st)$, where the growth rate is s, and $k = 2\pi/\lambda$ is the radial wavenumber. An algebraic eigenvalue problem proceeds for the growth rate: $\Sigma_{ij}\, z_j = s\, z_i$, where z_i is the eigenvector $(\hat{N}, u, v, \hat{P}_{xx}, \hat{P}_{xy}, \hat{P}_{yy}, \hat{P}_{zz})$ and Σ_{ij} is the 7×7 matrix governing the linear evolution of the system. Enforcing solvability returns a seventh-order dispersion relation subject to g, the equilibrium values of P_{ij} and the derivatives of Q_{ij}:

$$\begin{aligned}
&-s^7 + \mathsf{A}s^6 + (\mathsf{B}k^2 + \mathsf{C})s^5 + (\mathsf{D}k^2 + \mathsf{E})s^4 + (\mathsf{F}k^4 + \mathsf{G}k^2 + \mathsf{H})s^3 \\
&\qquad + (\mathsf{I}k^4 + \mathsf{J}k^2 + \mathsf{K})s^2 + (\mathsf{L}k^4 + \mathsf{M}k^2 + \mathsf{N})s + (\mathsf{P}k^4 + \mathsf{Q}k^2) \\
&+ g|k|\left(2s^5 + \mathsf{R}s^4 + (\mathsf{S}k^2 + \mathsf{T})s^3 + (\mathsf{U}k^2 + \mathsf{V})s^2 + (\mathsf{W}k^2 + \mathsf{X})s + \mathsf{Y}k^2\right) = 0.
\end{aligned} \tag{25}$$

The terms above are partitioned into those which occur independently of self-gravity (coefficients A–Q) and those which arise if it is included (R–Y). The coefficients are real and do not depend on g.

3.1.1 Viscous instabilities on long wavelengths

The analysis of (25) we initially limit to wavelike instabilities on large scales, $0 < k \ll 1$, i.e. wavelengths $\gg H$. And so as to capture how the various roots scale with wavenumber we expand s in $|k|$. For $s = \mathcal{O}(k^2)$,

$$s = -\frac{\mathsf{Q}}{\mathsf{N}}\, k^2 + \mathcal{O}(|k|^3), \tag{26}$$

which we identify as the potential viscous instability. Its criterion for instability can be determined from the sign of (Q/N), which is independent of the disk's self-gravity.

For $s = \mathcal{O}(1)$, Eq.(25) yields the sixth order polynomial equation,

$$-s^6 + \mathsf{A}s^5 + \mathsf{C}s^4 + \mathsf{E}s^3 + \mathsf{H}s^2 + \mathsf{K}s + \mathsf{N} = 0. \tag{27}$$

The quadratic $(1 + s^2)$ factors (27) on account of the two identities,

$$\mathsf{K} - \mathsf{E} + \mathsf{A} = 0, \qquad\qquad \mathsf{N} - \mathsf{H} + \mathsf{C} + 1 = 0 \tag{28}$$

(which may be verified by computer algebra). So, to leading order, two modes possess growth rates $s = \pm i$. These epicyclic oscillations we identify as the potentially overstable modes.

Without loss of generality we let $s = i + p|k| + qk^2 + \mathcal{O}(|k|^3)$ and return to (25), equating terms of order k. This obtains

$$\begin{aligned} p &= \frac{(\mathsf{V} - \mathsf{R}) + (\mathsf{T} - \mathsf{X} - 2)i}{(7 + 5\mathsf{C} - 3\mathsf{H} - \mathsf{N}) + (6\mathsf{A} - 4\mathsf{E} + 2\mathsf{K})i}\, g, \\ &= -ig. \end{aligned}$$

At order k^2 we collect the contributions to q from self gravity and find them equal to

$$-\frac{(15\mathsf{A} - 6\mathsf{E} + \mathsf{K} - 2\mathsf{V} + 4\mathsf{R}) + (-11 - 10\mathsf{C} + 3\mathsf{H} + \mathsf{X} - 3\mathsf{T})i}{(-7 + 5\mathsf{C} - 3\mathsf{H} + \mathsf{N}) + (6\mathsf{A} - 4\mathsf{E} + 2\mathsf{K})i}\, g^2 = -\frac{1}{2}\, i\, g^2$$

Computer algebra is required to establish both these identities. They reveal that the total effect of self-gravity on the overstable modes up to k^2 for $k \ll 1$ lies only in altering the wave frequency. The real part of s (emerging at order k^2) is unaffected. The criterion for overstability, in fact, depends on the sign of

$$\Delta = (\mathsf{J} - \mathsf{P} - \mathsf{D})(7 + 5\mathsf{C} - 3\mathsf{H} + \mathsf{N}) + (\mathsf{G} - \mathsf{B} - \mathsf{M})(6\mathsf{A} - 4\mathsf{E} + 2\mathsf{K}). \tag{29}$$

If $\Delta > 0$ the disk is viscously overstable.

These results mirror those of a viscous fluid disk in the long-wavelength limit, as studied by Schmit and Tscharnuter 1995, Spahn *et al.* 2000, and Schmidt *et al.* 2001. Similarly to a fluid disk we expect self-gravity to extend the range of parameters for which the viscous instability and overstability occur, when k takes intermediate values. Without self gravity the modes of longest wavelength are the most susceptible to both instabilities. But inclusion of self gravity can induce the instabilities on intermediate lengthscales, $\lambda_1 < \lambda < \lambda_2 < \infty$, as well, where both λ_1 and λ_2 are in the neighbourhood of the Jeans length.

3.1.2 Thermal Modes

In actual fact Eq.(28) represents the decoupling of the dynamic modes from the thermal modes at leading order when $k \ll 1$. This is because the $(1,1)$ minor of Σ_{ij} is

$$\begin{pmatrix} \mathbf{E} & \mathbf{0} \\ \mathbf{0} & \mathbf{T} \end{pmatrix} + \mathcal{O}(k) \tag{30}$$

where E_{ij} is the two-by-two 'epicyclic block' and T_{ij} is the four-by-four 'thermal block':

$$\mathbf{E} = \begin{pmatrix} 0 & 2 \\ -\frac{1}{2} & 0 \end{pmatrix}, \qquad \mathbf{T} = \frac{\partial(Q_{xx}, Q_{xy}, Q_{yy}, Q_{zz})}{\partial(P_{xx}, P_{xy}, P_{yy}, P_{zz})} + \begin{pmatrix} 0 & 4 & 0 & 0 \\ -\frac{1}{2} & 0 & 2 & 0 \\ 0 & -1 & 0 & 0 \\ 0 & 0 & 0 & 0 \end{pmatrix}.$$

We have partitioned the latter matrix into a collisional component, C_{ij} (the Jacobian), and a part incorporating the effects of rotation and shear, H_{ij}. We presume these components scale like $|\mathbf{C}|/|\mathbf{H}| \sim \omega_c/\Omega$, i.e. the hydrodynamic limit will be dominated by collisional processes, and the collisionless limit by the anisotropizing effects of rotation and shear. Note that, to leading order in k, Eq.(30) and the thermal partition also hold for a dense gas model in which the terms for collisional production of P_{ij} and collisional flux of momentum are arbitrary functions of N, P_{ij} and the rate of strain tensor.

The 4 modes associated with the thermal block T_{ij} include the energy mode, familiar from hydrodynamics (see Schmidt *et al.* 2001), and three others which emerge from the extra degrees of freedom arising from the anisotropy. In the collisioness limit, $|\mathbf{C}| \ll 1$, we find two modes with $s = \pm 2i + \mathcal{O}(|\mathbf{C}|)$, and two with $s = \mathcal{O}(|\mathbf{C}|)$. The former pair, oscillating at twice the epicyclic frequency, possess, to leading order, the eigenvectors $(0, 0, 0, 4, 2i, -1, 0)$ and $(0, 0, 0, -4, 2i, 1, 0)$. These correspond to a perturbation of the velocity ellipsoid which is comprised of the oscillation of the horizontal principal axes

perturbations, and their rotation with respect to the equilibrium orientation angle, δ. One of the $s = \mathcal{O}(|\mathbf{C}|)$ modes we presume coincides with the energy mode sketched at the end of Section 2.3. The other is a mode affiliated with the relaxation of anisotropy, the features of which cannot be determined until we specify Q_{ij}.

In the hydrodynamic limit the thermal modes, to leading order, depend solely on the collisional dynamics, their growth rates coinciding with the eigenvalues of C_{ij}. These cannot be ascertained until Q_{ij} is known; but if it is presumed that collisions work to destroy anisotropy then we might expect the four modes in this limit to correspond to the hydrodynamic energy mode plus three 'relaxation' modes which express the decay of the deviatoric parts of the stress. This assumption may then be employed to determine a plausible approximation to the collision term, which, in fact, reproduces the generic Krook model proposed by Shu *et al.* 1985 . This is clearer if we solve for C^2 and Π_{ij}, rather than the pressure tensor, P_{ij}, in which case we write $\widetilde{\Sigma}_{ij}\widetilde{z}_j = s\widetilde{z}_i$, where $\mathbf{z} = (\hat{N}, u, v, \hat{C^2}, \hat{\Pi}_{xx}, \hat{\Pi}_{xy}, \hat{\Pi}_{yy})$. First we adopt a simple model where the anisotropic parts of the stress decay independently of each other at the rate $\zeta_{\rm A}$ when in the collisional limit, but where the thermal energy mode decays at the rate $\zeta_{\rm T}$. Then the revised collision block, $\widetilde{C}_{ij}$ will take the simple form: $\widetilde{\mathbf{C}} = \mathrm{diag}(-\zeta_{\rm T}, -\zeta_{\rm A}, -\zeta_{\rm A}, -\zeta_{\rm A})$, which suggests the formula

$$Q_{ij} = \tfrac{2}{3}\, F(N, C) N C^2\, \delta_{ij} - G_{ij}(N, \Pi_{ij}),$$

where $(\partial_{C^2} F + F)_0 = \zeta_{\rm T}$, $G_{kk} = 0$ and $G^0_{ij} = -\zeta_{\rm A}\Pi^0_{ij}$. If Π_{ij} is small we may expand G_{ij} in Π_{ij} which reproduces a variant of SS85 (for which $\zeta_{\rm A} = \omega_c$ and $F = \omega_c(2 + \varepsilon^2)/3$). But as is argued in Shu *et al.* 1985 the magnitude of the relative motions of the particles should also impact on the rate of thermalisation; for example, gentle or glancing collisions randomise particle velocities less efficiently than violent head-on collisions. The importance of this detail may be approximately quantified by the magnitude of C (mediated by ε if preferred), which leads us to connect the rate of anisotropic relaxation to the velocity dispersion via the first column of $\widetilde{C}_{ij}$. The collisional block will hence be no longer diagonal, and then G_{ij} will be also a function of C. The formula which ensues for Q_{ij} is the generalisation of Shu *et al.*'s 'generic Krook model', with which it agrees to first order in anisotropy.

The vertical structure of the disk may introduce anisotropy into the collisional dynamics once vertical averaging is accomplished. In this case F and G_{ij} may depend on Π_{zz} as well.

3.2 SS85 Model Stability Analysis

We perturb about the steady state presented in Eq.'s (16)–(17), and then linearise and non-dimensionalise analogously to the previous section but with $\hat{C} = C_0\,\hat{C}^*$ and $\omega_c = \Omega_0\,\omega_c^*$. The stars will be henceforth dropped.

To compute the contribution from the perturbed collision term we expand both ε^2 and ω_c in Taylor series about C_0^2 and N_0 respectively. In doing so we have neglected any possible variation in the collision frequency due to changes in the disk thickness (refer to the discussion of Section 2.3), an approximation which simplifies the analysis. This introduces the parameters: e (cf. Eq.(20)) and

$$\omega_0' \equiv (d\ln\omega_c/d\ln N)_0.$$

If dense effects were properly included then a measure of the influence of non-local effects would appear in a third parameter, $R \equiv a\Omega/v_c$. But we assume it negligibly small. Moreover, there being no other velocity scale, all instances of v_c vanish in the non-dimensionalisation. Consequently, the perturbed, linearised and non-dimensionalized collision term specific to the SS85 model is

$$\hat{Q}_{ij} = \omega_0\left[\tfrac{1}{3}(\omega_0'+1)(\varepsilon^2-1)\,\delta_{ij} + \Pi_{ij}^0\right]\hat{N} + \tfrac{1}{3}\omega_0(\varepsilon^2 - 1 + \varepsilon^2\,e)\,\delta_{ij}\hat{C}^2 + \omega_0\hat{\Pi}_{ij}.$$

As in the general case we have an eigenvalue problem for the growth rate s, subject now to the three parameters: ω_0 which sets the equilibrium, and e and ω_0' which measure its linear response. The coefficients of the resulting characteristic polynomial in (25) are functions of these three and are listed in Appendix A.

The stability problem is more tractable than Eq.(25) threatens. In fact analytic stability criteria can be derived for every instability the system exhibits in the long (and short) wavelength limits. That said the dispersion relation could be simplified substantially if we put into use Eq.(14) and the average of (1), in which case $\omega_0' = 1$ and $e \approx -0.234, -0.20, -0.19$. But we leave these as free parameters. Firstly, doing so provides a means by which the collision frequency's enhancement by the disk's self-gravity can be included. This effect should ensure ω_c is superlinear in N and thus $3/2 > \omega_0' > 1$. Secondly, leaving ω_0' and e open frees the system to exhibit the viscous overstability.

3.2.1 The Viscous Instability

To begin we restrict the analysis to large scales, $0 < k \ll 1$, and suppose $s = \mathcal{O}(k^2)$. Given $e < 0$, it follows from (A.14) that $\mathsf{N} < 0$; so, from (26), the

criterion for instability is $\mathsf{Q} > 0$ which, on employing (A.16), obtains

$$\omega_0' > \frac{-e\,(1+\omega_0^2)(11+2\omega_0^2)}{18\omega_0^2 + e\,(1+\omega_0^2)(11-2\omega_0^2)}, \tag{31}$$

when $\omega_0 > \widetilde{\omega}$, where $\widetilde{\omega}$ is the nondimensionalised turning point of ν, introduced in (19). This assures us that the instability is indeed the kinetic analogue of the viscous instability: if we substitute the expression for our particulate disk's effective kinematic viscosity (Eq.(18)) into the hydrodynamic criterion for viscous instability,

$$\beta + 1 \equiv \left(\frac{1}{\nu}\frac{d(N\,\nu)}{d\,N}\right)_0 < 0,$$

we recover precisely (31). Moreover we find that the growth rate is

$$s = -(\mathsf{Q}/\mathsf{N})\,k^2 + \mathcal{O}(|k|^3) = -3\nu_0\,(\beta+1)k^2 + \mathcal{O}(|k|^3) \tag{32}$$

on using (A.16) and (A.14) again, which is exactly the growth rate of the viscous mode as computed by hydrodynamics.

Two curves of marginal viscous stability in the (ω_0, ω_0') plane are plotted in Fig. 2. They diverge as ω_0 approaches $\widetilde{\omega}$ from above, and asymptote to $\omega_0' = 1$ as $\omega_0 \to \infty$. A simple calculation demonstrates that for $e < -9/11$ a marginal curve will asymptote to 1 from above, and for $e > -9/11$ from below. In the hydrodynamic regime (for a dilute ring) we may make the identification $\omega_0' = -\beta + \mathcal{O}(\omega_0^{-2})$. Therefore the kinetic criterion of viscous instability recovers the familiar hydrodynamic criterion, $\beta < -1$.

When $e \to 0$, both the curves' turning point and $\tilde{\omega}$ drift to the origin, rendering more of parameter space unstable. At $e = 0$ the entire quadrant is unstable, which coincides with the energy instability sketched at the end of Section 2.4. On the other hand as $e \to -\infty$ (the isothermal limit) we find $\widetilde{\omega} \to \sqrt{11/2}$, a finite value.

Our discussion of ω_c's form at the end of Section 2.3 would suggest that appropriate values of ω_0' lie between 1 and 3/2. Thus $e > -9/11$ will ensure that such disks are viscously unstable for all collision frequencies above a critical value close to $\widetilde{\omega}$. A quick calculation shows this value to be $(-11e/(9+11e))^{1/2}$. The data offered by experiment suggest $e < -9/11$, and thus indicate a *dilute* disk composed of hard, icy boulders falls into this category.

As the assumption of diluteness fails in Saturn's rings (as discussed earlier), the validity of these stability predictions is unclear. In fact, theories and simulations of 'dense' and low-optical thickness equilibria suggest that the viscous instability should not appear (Araki and Tremaine 1986 and Wisdom and

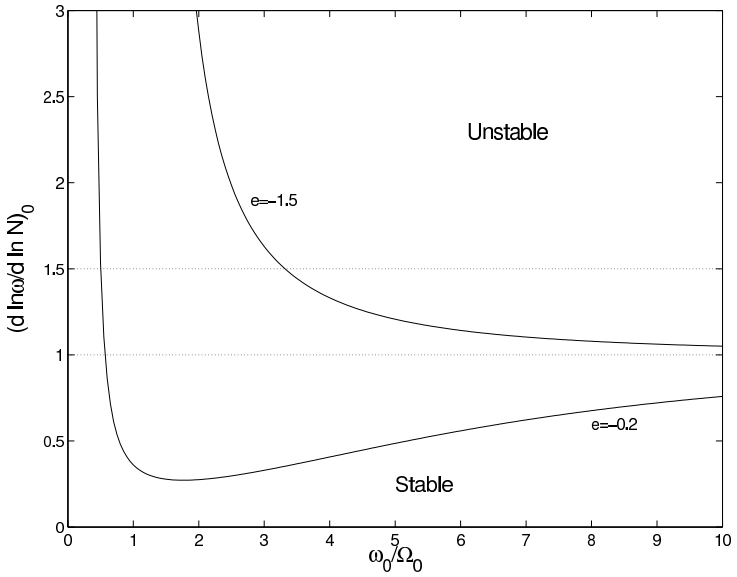

Fig. 2. Marginal Curves for the viscous instability in the (ω_0, ω_0') plane for $k \ll 1$ and different e representing the two regimes of $e > -9/11$ and $e < -9/11$. The regions above the curves are unstable. The dotted lines encompass the region $1 < \omega_0 < 3/2$ in which we expect to find equilibria characteristic of a dilute ring.

Tremaine 1988). Only in the simulations of Lukkari 1981 and Salo 2001 has the instability been observed, though the former used a scaling of the elasticity law which did not account for nonlocal effects, and the latter was for a 2D disk. So no physically realistic 3D simulation to date has exhibited the instability. This we presume is because either the parameters are not appropriate ($a\Omega/v_c$ or τ too big) or the lengthscales of the computations have not been sufficiently large to capture the unstable modes.

A final observation: if we let $\omega_0' = 1$ and solve for e we produce the stability criterion: $e > -(9/11)\omega_0^2/(1+\omega_0^2)$, which is qualitatively the same as that of Stewart *et al.* 1984 who solve a simplified kinetic model for only the optical thickness and thermal energy. So it appears that reduction is justified here.

3.2.2 The Viscous Overstability

In the long wavelength limit, $\Delta = 0$ describes the curves of marginal viscous overstability. Substituting the required coefficients obtains

$$\omega'_{\rm crit} = \frac{2(g_1 + g_2\, e + g_3\, e^2)}{9(1+\omega_0^2)(h_1 + h_2\, e + h_3\, e^2)} \tag{33}$$

where the g's and h's are the polynomials:

$$
\begin{aligned}
g_1(\omega_0) &= 9(-50886 - 75014\omega_0^2 - 24440\omega_0^4 - 1479\omega_0^6 + 139\omega_0^8 + 10\omega_0^{10}),\\
g_2(\omega_0) &= 6(990 + 5855\omega_0^2 + 9991\omega_0^4 + 6014\omega_0^6 + 959\omega_0^8 + 73\omega_0^{10} + 2\omega_0^{12}),\\
g_3(\omega_0) &= \omega_0^2(1+\omega_0^2)^2(-1851 - 1811\omega_0^2 - 100\omega_0^4 + 4\omega_0^6),\\
h_1(\omega_0) &= 9(-2178 + 833\omega_0^2 + 891\omega_0^4 + 156\omega_0^6 + 8\omega_0^8),\\
h_2(\omega_0) &= \omega_0^2(705 + 396\omega_0^2 - 351\omega_0^4 - 42\omega_0^6),\\
h_3(\omega_0) &= 2\omega_0^2(1+\omega_0^2)^2(-63 + 11\omega_0^2 + 2\omega_0^4).
\end{aligned}
$$

The modes are unstable when $\omega_0' > \omega_{\rm crit}'$, and the denominator in (33) negative (corresponding to $\omega_0 \gtrsim \widetilde{\omega}$); and when $\omega_0' < \omega_{\rm crit}'$, and the denominator positive ($\omega_0 \lesssim \widetilde{\omega}$). Thus the stability curve comprises two branches in the (ω_0, ω_0') plane, as plotted in Fig. 3.

The right branch approaches the line $\omega_0' = (\frac{2}{9} + \frac{2}{3}e^{-1})$ from below in the hydrodynamic limit, $\omega_0 \to \infty$, and only falls into the first quadrant of the (ω_0, ω_0') plane if $e < -3$. This is a value experiments show to be too low for hard ice particles. Moreover the maximum ω_0' for which overstability in the hydrodynamic limit is possible is 2/9. Thus a disk also needs to exhibit a strongly sublinear dependence of ω_c on N for overstability to develop, which is implausible. However, a number of formal results follow by making the identification $\beta = -\omega_0'$; we then obtain the hydrodynamic criterion $\beta > \beta_c = -(\frac{2}{9} + \frac{2}{3}e^{-1})$; and if, in addition, the isothermal limit, $e \to -\infty$, is enforced, we recover precisely the overstability criterion of Schmit and Tscharnuter for an isothermal fluid disk without bulk viscosity: $\beta > -2/9$.

The left branch is associated with the monotonically increasing dependence of equilibrium viscosity with N when $\omega_0 < \widetilde{\omega}$. Fig. 3 shows these curves to diverge when $\omega \approx \widetilde{\omega}$, and intersect the $\omega_0 = 0$ axis at a finite value of ω_0', which some algebra reveals to be $514/99 - (20/297)e$. Subsequently the minimum ω_0' for which left-branch viscous overstability is possible is ≈ 5.192— a highly superlinear dependence of ω_c on N. It follows that for all ω_0 and e there exists a 'channel', $2/9 < \omega_0' < 5$, in which overstability is forbidden. The equilibria of a dilute ring lie well within this region, hence viscous overstability will not occur in a dilute ring.

3.2.3 Thermal Modes

We complete the $k \ll 1$ analysis by examining the four modes embodied in the SS85 thermal block $\widetilde{\mathbf{T}}$, analogous to that appearing in Eq.(30). We find that the cooling component of this matrix is the expected, $\widetilde{\mathbf{C}} = \mathrm{diag}(-\Gamma_{C^2}, -\omega_0, -\omega_0, -\omega_0)$, where we have defined the collisional cooling rate to be $\Gamma \equiv \frac{1}{2}C^2 N\omega_c(1-\varepsilon^2)$, and the subscript C^2 indicates partial differentiation with respect to squared velocity dispersion.

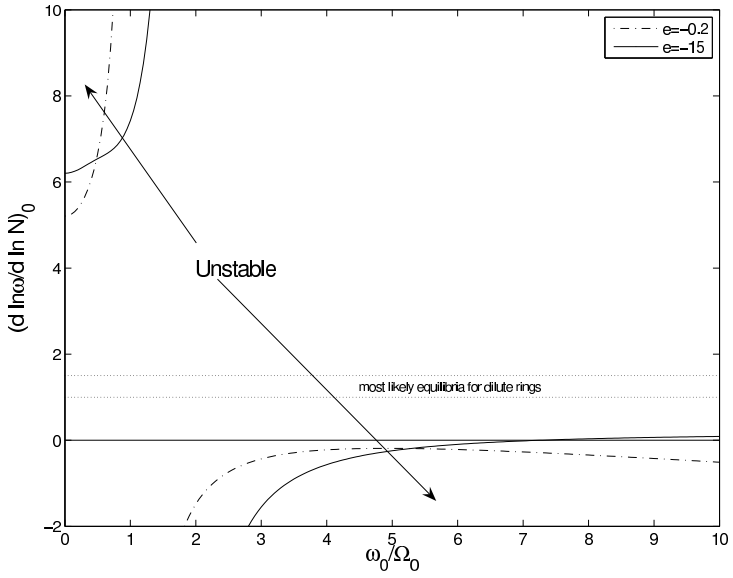

Fig. 3. The two branches of the marginal curves of viscous overstability in the (ω_0, ω_0') plane for different e and with $k \ll 1$. The left branch intersects the $\omega_0 = 0$ axis at $\omega_0' = 514/99 - (20/297)e$, and the right branch asymptotes to the line $\omega_0' = (\frac{2}{9} + \frac{2}{3}e^{-1})$. Probable values of ω_0' lie in the dotted channel $1 < \omega_0' < 3/2$.

In the hydrodynamic limit, $\omega_0 \to \infty$, the heating contribution to $\widetilde{\mathbf{T}}$ is subdominant and the stress components, Π_{xx}, Π_{xy} and Π_{yy} possess (to leading order) a decay rate equal to ω_0 (representing the 'relaxation modes'), while the velocity dispersion, C^2, decays at the rate Γ_{C^2} (corresponding to the mode in which the energetic stability of the equilibrium is expressed).

In the converse collisionless regime, $\omega_0 \ll 1$, we recover the complex conjugate pair we met earlier. Their growth rates are

$$s = \left[\pm 2i - \tfrac{1}{176}(100 + e)\omega_0 + \mathcal{O}(\omega_0^2)\right] + \mathcal{O}(|k|),$$

and so are stable for all $e > -100$, an upper bound which is much larger than the values of e we deem feasible. These two modes are analogous to those of the viscous overstablity, only becoming unstable when the thermal restoring forces are sufficiently strong (i.e. e negative and large). The mechanism animating them we presume works to quench perturbations of the horizontal axes of the velocity ellipsoid, but may be so effective that the resulting 'overshoot' may instigate an oscillation of growing amplitude. The instability can therefore be thought of as an 'anisotropic overstability'.

For general ω_0 there is a single 'relaxation mode' with growth rate $s = -\omega_0 + \mathcal{O}(|k|)$, composed exclusively of Π_{xx} and Π_{yy} perturbations in the ratio 4 to 1. This mode deforms the velocity ellipsoid, either vertically squashing or vertically dilating it, but while maintaining C constant. Thus it is a pure rearrangement of anisotropy. Factoring out this mode from the characteristic polynomial of $\widetilde{T}_{ij}$ leaves a cubic in s with a single real solution corresponding

to the growth rate of the energy mode. This is negative if:

$$\tfrac{1}{3}\omega_0(11+2\omega_0^2)\left[\Gamma_{C^2}-\tfrac{9}{4}\left(\frac{2\omega_0}{11+2\omega_0^2}\right)\right]>0. \tag{34}$$

The square bracketed term we identify as the partial derivative of the energy balance with respect to squared velocity dispersion, C^2, because it is composed of the derivative of the collisional cooling function, Γ, and the viscous heating, $\frac{9}{4}\nu_0$. Thus thermal stability on large scales depends solely on the response of the energy equilibrium to small fluctuations in velocity dispersion. When we substitute Γ_{C^2} into Eq.(34) the condition simplifies to $e<0$, which justifies the heuristic argument offered at the end of Section 2.4.

3.2.4 Instabilities on Intermediate Lengthscale

Now we solve for general k. Caution should be exercised in interpreting the results of this analysis, considering the omission of the third order moments. These will certainly dominate short-scales but should also play some part on intermediate lengths. We will discuss their effects in more depth in the hydrodynamic analysis of Section 4.

Let us begin without self-gravity, i.e. let $g=0$. We seek the marginal stability of non-oscillatory modes, and hence let $s=0$. The curves of marginal stability for a mode of wavenumber k are determined by

$$\mathsf{P}k^2+\mathsf{Q}=0,$$

which derives from Eq (25). The criterion $\mathsf{Q}=0$ describes the marginal stability of the longest waves and coincides with the criterion of viscous instability. The criterion $\mathsf{P}=0$ corresponds to marginal stability on the shortest wavelengths, and is associated with an energy mode. Because we assume $e<0$ thermal stability will hold on long wavelengths (see the analysis in Section 3.2.3) but on shorter scales this need not be true. Outside the long wavelength regime density perturbations can no longer be factored out and the energy balance's dependence on N plays a part. We shall discover in the hydrodynamic analysis that this energy mode attempts to keep both pressure and viscous stress constant, and its stability is related subsequently to Field's criterion (Field 1965) . That said the omitted terms representing the heat flux we presume enter at higher order than k^2 and should extinguish this instability on sufficiently short scales. On intermediate scales instability is guaranteed if $\mathsf{Q}/\mathsf{P}<0$, which refers to a hybrid mode of viscous and thermal effects. Again, omission of the third order moments will probably affect its stability.

With self-gravity added the curves of marginal stability for a non-oscillatory

mode are described by

$$\mathsf{P}\,k^2 + \mathsf{Y}g\,|k| + \mathsf{Q} = 0.$$

Solvability for $|k|$ furnishes the criterion $g^2 > g^2_{\rm crit} \equiv 4\mathsf{QP}/\mathsf{Y}^2$, or equivalently, $Q < Q_{\rm crit}$, where Q is the Toomre parameter. The critical value $g_{\rm crit}$ is a complicated function of ω_0, ω_0' and e, which we list in (B.1).

In Fig. 4 curves of marginal stability are plotted in (ω_0, ω_0') space for $g = 1$ and $e = -0.2$. Three curves are plotted. Equilibria in the region above the dotted graph will develop *viscous instability* on all wavelengths above a critical lengthscale. This is precisely the same curve we encountered in the long wavelength analysis, as the most unstable wavelengths are the longest. The solid graph represents marginal *viscous/gravitational instability*, above which equilibria become unstable. The unstable region includes that of the viscous instability, which is a special case. Modes which are viscous/gravitationally unstable possess wavelengths in an interval (λ_1, λ_2) bracketing the Jeans length; modes which are viscously unstable possess $\lambda_2 = \infty$. The marginal curve of viscous/gravitational instability asymptotes to a line $\omega_0' = 1 - g^2/3$ for ω_0 large, a fact easily verified from Eq.(B.1). It follows that in the hydrodynamic limit the instability criterion can be written as $\beta < \beta_c = -(1 - g^2/3)$, which agrees with Schmit and Tscharnuter's criterion (Eq.(35) in Schmit and Tscharnuter 1995) for an isothermal disk. This fact suggests that the thermal properties of the ring play a negligible role on the stability criterion of the most unstable mode in the collision-dominated, hydrodynamic limit.

The dotted-dashed curve in Fig. 4 represents the *quasi-thermal instability*, which affects all modes with wavelengths *below* a critical intermediate value. Perhaps we can then characterise it, like the viscous instability, as a special case of gravitational/viscous instability but in which $\lambda_1 = 0$. Inclusion of a heat flux term would undoubtedly prevent λ_1 being zero. So in reality scales sufficiently small will be stable.

Suppose that we take $\omega_0' = 3/2$, $e = -0.234$ and $g = 1$. For k small the SS85 model predicts that viscous instability will be present in those parts of a dilute ring in which there are more than 3.5 collisions per orbit (i.e. $\omega_0 \gtrsim 0.555$), a critical limit which corresponds to an optical thickness of 0.218 if we employ expression (14). If, however, we include ω_c's self-gravity factor, introduced in equation (15), the viscous instability can occur for lower optical thicknesses; for example if $g = 1$ instability occurs for $\tau > 0.089$. Hence only the most tenuous of dilute rings will be stable.

The SS85 model also suggests that on intermediate scales quasi-thermal or viscous/gravitational instability will occur in parts of the ring in which there are less than about 33 collisions per orbit ($\omega_0 \lesssim 5.2318$), which corresponds to a critical τ of approximately 2 (or less if ω_c's self-gravity factor is included). This last result is dubious, of course, because of the omission of the third

order moments. The prevalence of quasi-thermal and viscous/gravitational instability on intermediate scales is a question left open until the next section.

We will not undertake an analogous analysis of the viscous overstability in the intermediate range, it being algebraically intensive and not especially illuminating. In summary, the inclusion of self gravity narrows the 'channel of stability' in the (ω_0, ω_0') plane, but not sufficiently to endanger the stability of equilibria with appropriate values of ω_0'. Instability on those regions of parameter space rendered 'newly' unstable by self-gravity disturb modes on intermediate scales only; thus the 'old' boundaries of stability circumscribe regions in which viscous overstability operates on arbitrarily long wavelengths.

It should be mentioned that in the $k \gg 1$ regime the system not only evinces the unphysical extension of the quasi-thermal instability but also two pairs of unstable sound waves, which we also regard as unphysical. That said these only appear for parameter values incongruent with a dilute ring of icy particles: the first pair of modes may only be unstable when $e < -65$, and the second when $\omega_0' < 0.98$ for e and ω_0 sufficiently small. Thus the thermal instability will be the primary problem if one sought to undertake a non-linear computation of the time-dependent equations.

4 Comparison with Viscous Fluid Disk

In this section we compare the linear analysis of our kinetic system with that of hydrodynamics. The motivation for doing so is to distinguish the effect of the viscous stress equation, which should not only capture anisotropic effects but also the non-Newtonian behaviour of the stress in the range of low and intermediate ω_0. We produce an analysis analogous to Schmidt *et al.* 2001, and thus solve the mass conservation equation, the Navier-Stokes equation, the temperature equation and Poisson's equation for a self-gravitating, viscous fluid disk in a shearing sheet. We omit however Schmidt *et al.*'s nonlocal contributions to pressure and viscosity. So as to best mimic our kinetic disk the transport coefficients have been set to those computed by the SS85 kinetic equilibrium. Hence the coefficient of bulk viscosity and heat diffusivity, κ, are zero for the moment, the latter corresponding to the omission of the third order moments. The shear viscosity is

$$\nu = \frac{2\omega_c(N)\, T}{11\Omega_0^2 + 2\omega_c(N)^2}, \tag{35}$$

where $T \equiv C^2$ is temperature. In addition we incorporate the 'cooling function', Γ, into the temperature equation which shall account for collisional

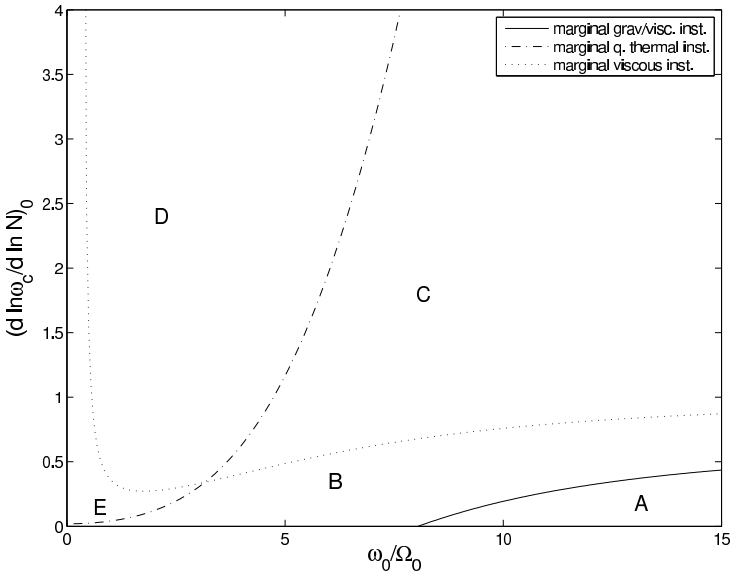

Fig. 4. Marginal Curves for the viscous instability, quasi-thermal instability and viscous/gravitational instability for general k in the (ω_0,ω_0') plane for $e = -0.2$ and $g = 1$, as predicted by the SS85 kinetic model. Regions above the curves are unstable. Thus equilibria in Region A are stable. Region B circumscribes equilibria susceptible to gravitational/viscous instability on modes with $k \in (k_1, k_2)$. Equilibria in Region C feature viscous instability affecting modes with $k < k_3$. In Region D both quasi-thermal instability and viscous instability are apparent, and so every mode is unstable. And in Region E both quasi-thermal and gravitational/viscous instability exist on all wavenumbers greater than a critical value k_4. The curve of viscous instability asymptotes to $\omega_0' = 1$ for large ω_0, while the curve of viscous/gravitational instability goes to $\omega_0' = 1 - g^2/3$.

energy losses,

$$\Gamma = \tfrac{1}{2}\omega_c \, N \, T \, (1 - \varepsilon(T)^2). \tag{36}$$

The fluid equations in the shearing sheet read:

$$\begin{aligned} D_t N &= -N \partial_k u_k, \\ N \, D_t u_i &= -N \, \partial_i (\Phi_P + \Phi_D) - \partial_i P + \partial_k \Pi_{ik}, \\ \tfrac{3}{2} \, N \, D_t \, T &= -P \, \partial_k \, u_k + \Psi - \Gamma, \end{aligned}$$

where pressure is defined by $P \equiv NT$ and the rate of viscous heating is $\Psi = \Pi_{kl} S_{kl}$, where $S_{ij} = e_{ij} - \partial_k u_k \delta_{ij}/3$ designates the rate of deformation tensor. The stress is Newtonian, so $\Pi_{kl} = 2N\nu S_{kl}$, and Φ_D is determined from Poisson's equation (12). It is understood these equations, and the fields which appear in them, are vertically averaged.

The stationary state is represented by: the equilibrium surface number density N_0, the Keplerian shear $\mathbf{u} = -\frac{3}{2}\Omega_0 \, x \, \mathbf{e}_y$, and the equilibrium temperature T_0, which is computed from the energy balance. We perturb, linearise and non-dimensionalise this state as earlier, expanding both ν and Γ in Taylor series. On assuming wavelike perturbations $\propto e^{st+ikx}$ the system yields the

non-dimensional fourth-order dispersion relation:

$$
\begin{aligned}
& s^4 + \{E_{\rm T} + \tfrac{7}{3}\nu k^2\}\, s^3 \\
& \qquad + \{1 - 2g|k| + (\tfrac{5}{3} + \tfrac{10}{3}E_{\rm T}\nu_0 + 3\nu_{\rm T}\,\nu_0)k^2 + \tfrac{7}{3}\nu_0^2\, k^4\}s^2 \\
& + \{E_{\rm T}(1 - 2g|k|) + (E_{\rm T} - \nu_0 + 2\nu_{\rm T}\left[\tfrac{9}{2}(1+\xi)\nu_0 - \tfrac{2}{3}\Gamma_{\rm N}\right])k^2 \\
& \qquad - 2g\nu_0\,|k|^3 + (\tfrac{7}{3}E_{\rm T}\nu_0 + 7\nu_{\rm T}\nu_0 + \tfrac{5}{3})\nu_0 k^4\}\, s \\
& + \{2(1+\xi)\Gamma_{\rm T} - 2\Gamma_{\rm N}\nu_{\rm T}/\nu_0 - 2g\,(\tfrac{2}{3}\Gamma_{\rm T} + \tfrac{3}{2}\nu_{\rm T})\,|k| \\
& \qquad + \left(\tfrac{2}{3}(\Gamma_{\rm T} - \Gamma_{\rm N}) - \tfrac{3}{2}(1+\xi)\nu_0 + \tfrac{3}{2}\nu_{\rm T}\right)k^2\}\nu_0\, k^2 = 0, \qquad (37)
\end{aligned}
$$

where $\xi \equiv (\partial \ln \nu/\partial \ln N)_0$, $\nu_T = (\partial\nu/\partial T)_0$, and $E_{\rm T} = \frac{2}{3}(\Gamma_{\rm T} - \Psi_{\rm T})$ which is 2/3 times the partial derivative of the system's net rate of cooling with respect to temperature. Note that ξ is a partial derivative and thus differs from β introduced in Section 1. If heat diffusivity κ is included other terms materialise, the ones of relevance to our analysis being:

$$\nu_0\, k^2(\tfrac{2}{3}\kappa k^4 - \tfrac{4}{3}g\kappa|k|^3 + 2(\xi+1)\kappa k^2).$$

For more details see Schmidt *et al.* 2001.

In order to complete the linear theory of the fluid analogue we replace the four extra parameters appearing in the dispersion relation with

$$\Gamma_{\rm N} = \frac{9\omega_0\,(1+\omega_0')}{2(11+2\omega_0^2)}, \qquad \Gamma_{\rm T} = \tfrac{1}{2}\omega_0\,\frac{9 - 2e(1+\omega_0^2)}{11+2\omega_0^2}, \qquad (38)$$

$$\xi = \omega_0'\,\frac{(11-2\omega_0^2)}{(11+2\omega_0^2)}, \qquad \nu_{\rm T} = \frac{2\omega_0}{11+2\omega_0^2}. \qquad (39)$$

4.1 Modes on Large Lengthscales

In the long-wavelength limit, $k \ll 1$, and assuming $s = \mathcal{O}(k^2)$, the viscous mode has growth rate:

$$s = -2\,\frac{(1+\xi)\Gamma_{\rm T}\nu_0 - \Gamma_{\rm N}\nu_{\rm T}}{E_{\rm T}}\,k^2 + \mathcal{O}(k^3)$$

On applying Eq.'s (38)–(39), curves of marginal viscous instability are derived which are identical to those predicted by the kinetic model in Eq.(31). Also if we let $s = \mathcal{O}(1)$ we find the long-wavelength thermal mode:

$$s = -E_{\rm T} + \mathcal{O}(k^2).$$

which reproduces Eq.(34).

The growth rate of an overstable mode Schmidt *et al.* show to be

$$s = i - ig|k| + \tfrac{1}{2}(\gamma_i - g^2)ik^2 + \tfrac{1}{2}(\gamma_r + \tfrac{2}{3}\nu_0 + 3\xi\nu_0)k^2,$$

where

$$\gamma_i = -\frac{1}{1+E_{\rm T}^2}\left[\left(\frac{2}{3}\Gamma_{\rm N}\,E_{\rm T} - \frac{1+3\xi}{2}\,\nu_0\,E_{\rm T} - \frac{2}{3}\right) + 3\nu_{\rm T}\left(\frac{2}{3}\,\Gamma_{\rm N} - \frac{(1+3\xi)}{2}\,\nu_0 + \frac{2}{3}\,E_{\rm T}\right)\right],$$

$$\gamma_r = -\frac{1}{1+E_{\rm T}^2}\left[\left(\frac{2}{3}\Gamma_{\rm N} - \frac{1+3\xi}{2}\,\nu_0 + \frac{2}{3}\,E_{\rm T}\right) - 3\nu_{\rm T}\left(\frac{2}{3}\Gamma_{\rm N}\,E_{\rm T} - \frac{1+3\xi}{2}\,\nu_0\,E_{\rm T} - \frac{2}{3}\right)\right],$$

in the absence of nonlocal terms. Hence the curves of marginal overstability proceed from

$$\xi_{\rm crit} = \xi^* \equiv \frac{-4\Gamma_{\rm N} - 4E_{\rm T} + 7\nu + 4E_{\rm T}^2\nu_0 + 3\nu_{\rm T}(4 - 4E_{\rm T}\Gamma_{\rm N} - 3E_{\rm T}\nu_0)}{9\nu_0(3 + 2E_{\rm T}^2 + 3E_{\rm T}\,\nu_{\rm T})}.$$

which translates, in the parameters of our dilute ring, to

$$\omega'_{\rm crit} = \frac{(11+2\omega_0^2)(l_1 + e\,l_2 + e^2\,l_3)}{9(l_4 + e\,l_5 + e^2\,l_6)}, \tag{40}$$

where

$$\begin{aligned} l_1 &= 45(11+2\omega_0^2)^2, & l_2 &= 6(121 + 183\omega_0^2 + 66\omega_0^4 + 4\omega_0^6),\\ l_3 &= 8\omega_0^2(1+\omega_0^2)^2, & l_4 &= 9(-1331 + 132\omega_0^4 + 16\omega_0^6),\\ l_5 &= -72\omega_0^4(1+\omega_0^2), & l_6 &= 4\omega_0^2(-11+2\omega_0^2)(1+\omega_0^2)^2. \end{aligned}$$

These curves resemble roughly those of the kinetic model, consisting of two branches: one tightly bunched near the collisionless limit and one which extends over the remainder of parameter space (See Fig. 5). In the limit $\omega_0 \to \infty$ the graphs asymptote, like the kinetic curves, to $\omega'_0 = (\frac{2}{9} + \frac{2}{3}e^{-1})$. However for intermediate and lower values of ω_0 the two accounts disagree markedly. The kinetic and fluid graphs diverge at different values of the collision frequency, ω_0. And the left branch intersects the $\omega_0 = 0$ axis at $\omega'_0 \approx -0.556 - 0.074e$. Hence for $e > -1.874$ overstability occurs for all ω'_0 to the left of the singularity. This contradicts the kinetic model which predicts that no viscous overstability can occur for $2/9 < \omega'_0 < 5.192$. Thus a dilute ring of icy particles with $e = -0.234$, $\omega'_0 = 3/2$, and $g = 1$ manifests viscous overstability for all $\omega_0 < 2.2022$, or $\tau < 0.541$

This is an important qualitative difference, and which we argue results from the non-Newtonian nature of the viscous stress, in particular its nonlocality

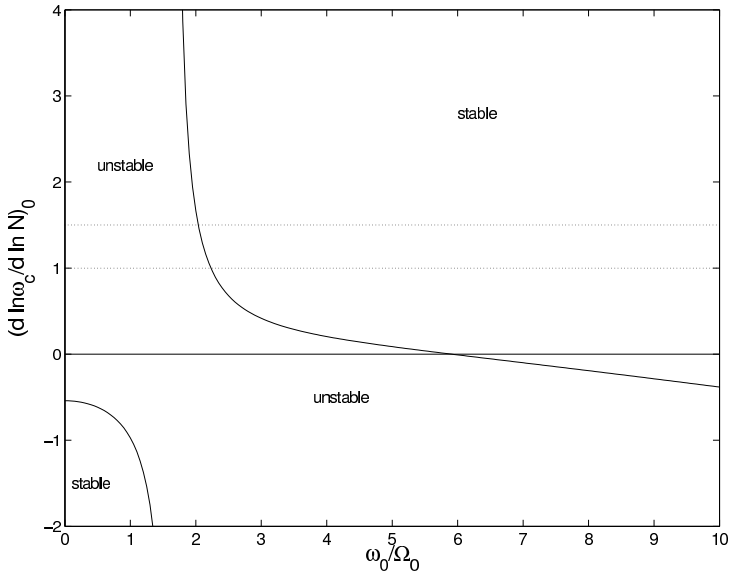

Fig. 5. Marginal curve of viscous overstability predicted by hydrodynamics for $e = -0.2$ and $k \ll 1$. The right branch asymptotes to the line $\omega_0' = 2/9 + 2/(3e)$, for large ω_0 (in agreement with the kinetic model) but diverges to $+\infty$ for an intermediate value of ω_0, as opposed to the kinetic model which diverges to $-\infty$. The left branch differs markedly, intersecting the $\omega_0 = 0$ axis for negative ω_0' and thus ensuring a large sector of parameter space is unstable. The channel $1 < \omega_0' < 3/2$ indicates the region in which we expect appropriate equilibria to fall.

in time. This effect interferes with the phase synchronisation of the stress and density oscillations, and thus the mechanism sustaining the overstable modes. It is less clear how anisotropy is at work here, but we conclude it plays a smaller effect in the linear theory. This effect we expect to be less appreciable for a dense gas, as the collisional contribution to the viscous stress, which is local in time, will be of order or greater than the free-streaming component, which is non-local in time.

4.2 General Stability Criterion for Non-Oscillatory Modes

We derive a relation describing the marginal stability of non-oscillatory modes from (37) if we set $s = 0$. It follows that instability occurs on an interval of k if the following equation admits two solutions for $|k_c|$,

$$\left[\tfrac{2}{3}(\Gamma_{\rm T} - \Gamma_{\rm N}) - \tfrac{3}{2}(1+\xi)\nu_0 + \tfrac{3}{2}\nu_{\rm T}\right] k_c^2 - 2g\,\left[\tfrac{2}{3}\Gamma_{\rm T} + \tfrac{3}{2}\nu_{\rm T}\right] |k_c| + [2(1+\xi)\Gamma_{\rm T} - 2\Gamma_{\rm N}\nu_{\rm T}/\nu_0] = 0, \qquad (41)$$

Eq.(41) is the counterpart of (32), the coefficients of k_c^2, $|k_c|$ and k_c^0 corresponding to P, Y and Q, respectively. Thus the coefficient of k_c^0 determines the onset of viscous instability and dominates in the long wavelength limit. The coefficient of $|k_c|$ introduces self-gravitation. The coefficient of k_c^2 mani-

fests thermal effects, and is in fact equal to the derivative of 2/3 times the net rate of cooling, $E = \frac{2}{3}(\Gamma - \Psi)$, with respect to temperature, if *both* pressure and the viscous stress are kept constant. To show this we must include the variations induced by temperature and density displacements upon the shear rate, A, which compensates for the variation in ν induced by the same perturbations. If Π_{xy} is to be kept constant, given a fluctuation in N and T at constant P, then

$$\frac{\partial A}{\partial T} = \tfrac{3}{2}\left[\nu_{\rm T}/\nu_0 - (1+\xi)\right],$$

and therefore

$$\left(\frac{\partial E}{\partial T}\right)_{P,\,\Pi_{xy}} = \tfrac{2}{3}(\Gamma_{\rm T} - \Gamma_{\rm N}) - \tfrac{3}{2}(1+\xi)\nu_0 + \tfrac{3}{2}\nu_{\rm T}.$$

It follows that the criterion for quasi-thermal instability on very short scales (when Eq.(41) is dominated by the thermal term) is a modification of Field's criterion $(\partial E/\partial T)_P < 0$ (Field 1965). But on intermediate scales, the potentially unstable mode will be an amalgam of effects associated with the thermal balance, self-gravitation and angular momentum transport, all constrained to maintain constant pressure and stress.

The marginal curves which follow from Eq.(41) match those of SS85 (described in Fig. 4); the viscous/gravitational graph nearly coincides, and the quasi-thermal graph is qualitatively the same. Here the discrepancies which do exist between the two models we attribute to the breakdown of the assumptions of both on intermediate scales. Their details we omit.

Heat diffusivity introduces the additional terms $-\frac{4}{3}g\kappa|k|^3 + \frac{2}{3}\kappa k^4$ which contribute at sufficiently small scales. Including heat conduction will also incur a k^2 term, $2(\xi+1)\kappa k^2$, representing the coupling of thermal transport with rotation and viscosity. Hence the criterion of intermediate scale instability will be altered significantly. This may be quantified by a critical heat diffusivity, $\kappa_{\rm crit}$ below which quasi-thermal instability can emerge on a band of k, the upper limit depending sensitively on κ. An expression for this quantity in the non-self-gravitating case is presented in Eq.(C.1). We find this critical value to be very small indeed; for instance, when $e = -0.234$, $\omega_0' = 1$ and $\omega_0 \lesssim 0.7$ then $\kappa_{\rm crit} \lesssim 0.07$. The dilute kinetic theory asserts that $\nu \sim \kappa$ (Cowling and Chapman 1970), so for (35) only dilute rings of large optical thicknesses ($\tau \gtrsim 3$) should feature the quasi-thermal instability.

When the destabilising effect of self-gravity is added, however, $\kappa_{\rm crit}$ can approach feasible values. Instability in this case we name viscous/gravitational, though in fact the mode in question is fueled by viscous, gravitational and thermal processes. In order to establish how this instability impacts on the various scales we plot curves of marginal stability in the (ω_0, ω_0') plane for given e, κ and k, as described by Eq.(C.2) (Fig. 6). When $\kappa \lesssim 1$ we find that

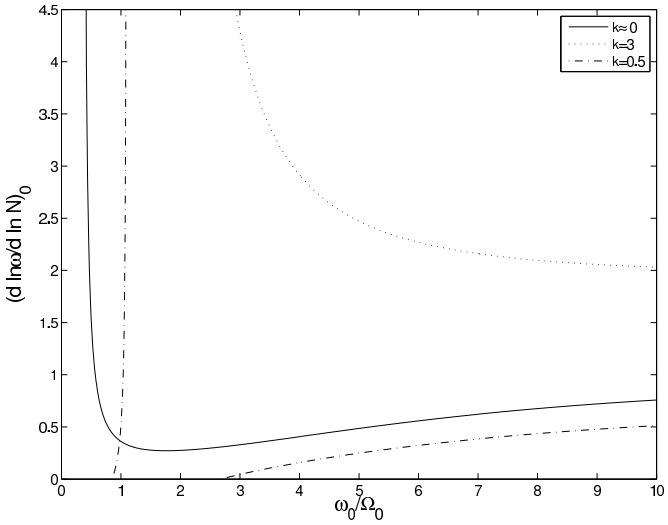

Fig. 6. Marginal curves of non-oscillatory instability for three representative values of k as predicted by the hydrodynamical model, when $e = -0.2$, $g = 1$, and $\kappa = 1$. Equilibria situated above the $k \approx 0$ curve are unstable on the longest scales, but those above the $k = 3$ curve are stable for scales $k > 3$. Marginal curves for larger k disappear into the top right. The area outside the region bounded between the two branches of the dotted-dashed curve are stable on scales $k > 0.5$

the marginal curves fall into three categories corresponding to long, intermediate and short scales. For scales $k < k_{1c}$ we obtain curves resembling those of viscous instability (see Fig. 2). But for scales $k_{1c} < k < k_{2c}$ there appear two branches, the right one familiar from Fig. 4, the left arising from non-zero κ. Instability emerges on equilibria situated between the two. We conclude that heat diffusion confines instability on intermediate scales to a smaller area of parameter space than predicted otherwise; in particular, equilibria with low ω_0 are stabilised. For short waves, $k > k_{2c}$, the marginal curves mimic in shape those of long wavelength, but as k gets large $\omega'_{\rm crit} \gtrsim k^2$. Therefore if small scales are to be rendered unstable the system needs to exhibit an inappropriately large value of ω'_0. As expected, heat diffusivity stabilizes short scales. Expressions for k_{1c} and k_{2c} may be obtained by examining the real roots shared by the numerator and denominator of (C.2). For $\kappa = 1$, they are approximately equal to $g \pm \sqrt{g^2 - (6/11)\widetilde{\omega}}$, which lie on either side of half the Jeans length. The fluid model then predicts that a dilute ring, with self gravity ($\omega'_0 = 3/2$) and $\kappa = 1$, is stable on scales $\lambda^* < 2\pi\sqrt{2/3}$, or about 5 times the disk semi-thickness.

It is likely a kinetic theory, accounting for heat conductivity adequately, would predict similar results, though this cannot be checked until such a model is devised. However, hydrodynamics shows clearly that if we wish to study behaviour on intermediate and short scales, it is necessary to include in some way the third-order moments.

5 Comparison with the Goldreich & Tremaine Kinetic Model

This section outlines the linear stability of the GT78 model, so as to compare the modified Krook collision term with that of a formal Boltzmann-type account.

Goldreich and Tremaine take the distribution function, f, to be a three-dimensional Gaussian in velocity space with its axes corresponding to the principal axes of the pressure tensor, p_{ij}. Assuming symmetry about the plane $z = 0$, the principal axis system is denoted by the unit vectors $\mathbf{e}_1$, $\mathbf{e}_2$ and $\mathbf{e}_3 = \mathbf{e}_z$, so that $\mathbf{e}_z \sin\delta = \mathbf{e}_x \times \mathbf{e}_1$, where δ denotes the orientation angle. The principal values of p_{ij} are accordingly defined by $p_{kk} = n\, c_k^2$, where $k = 1, 2, 3$, and the summation convention is not applied. The velocity distribution is then

$$f(\mathbf{v}) = \frac{n}{(2\pi)^{3/2} c_1 c_2 c_3} \exp\left(- \sum_{k=1}^{3} \frac{v_k^2}{2 c_k^2} \right). \tag{42}$$

This form results in a much simplified collision term; see Eq (33) in GT78. However to facilitate better the comparison with SS85, we assume the value of ε, which appears in the collisional kinematics, is a quantity averaged over collisions, and not a constant. Also we note that the implicit collision frequency in the resulting Q_{ij} is $\propto \Omega\tau\, c_k/c_3$ and thus is dependent on the velocity dispersions, being 'weighted' differently for each direction. It does not capture self gravity or filling factor effects in its present form– these requiring a superlinear dependence on τ.

5.1 Equilibrium Solution

For the equilibrium analysis we solve the four components of the pressure tensor equation (10) in the principal axis frame, cf. Eqs (37) in GT78. Given τ, these determine ε, δ, and the axis ratios of the velocity ellipsoid, c_2/c_1 and c_3/c_1.

The results of our numerical root finding reproduce those of GT78 and can be observed in Fig. 7, in which we plot the $\varepsilon - \tau$ law only. The SS85 relationship is plotted for comparison. Eq.(14) has been used to relate τ and ω_c. As mentioned earlier the discrepancy at low τ is marked. For more discussion of this see SS85 and Shu *et al.* 1985.

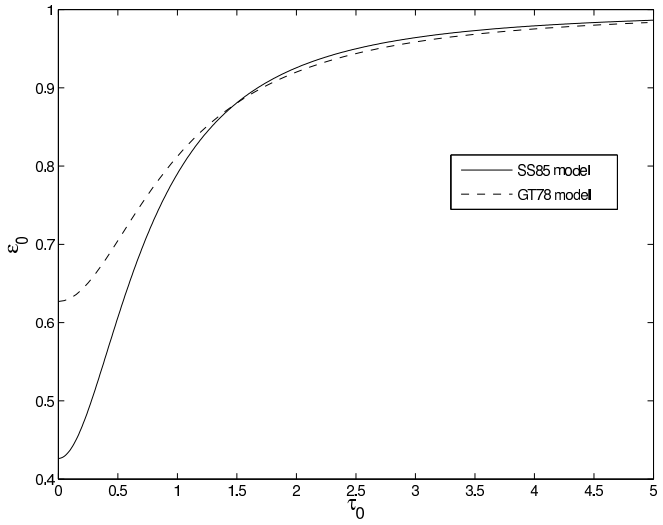

Fig. 7. The energy equilibrium relations between the coefficient of restitution, ε_0, and optical thickness, τ_0, as determined by the SS85 and GT78 models.

5.2 The GT78 Linear Stability

In order to model the action of self gravity on the collision frequency we re-parametrise the disk equilibrium and replace optical thickness by ω_0, as expressed in (14). For the purposes of the linear stability analysis we then treat ω_c as a superlinear function of N. This we admit is somewhat crude but should approximate to an acceptable degree self-gravity's enhancement of the collision frequency, and certainly sharpen the comparison with the SS85 model.

We now perturb about the steady state calculated in the previous section. We then linearise and non-dimensionalise, though on account of the complicated form of the collision term this process is rather involved:

(1) First, we must calculate, in the principal axis frame, the three collision term perturbations, $\hat{Q}_{kk}$, in terms of perturbations of τ, δ, and the principal velocity dispersions, c_k.
(2) Then the c_k and δ perturbations are converted to those of the $\hat{P}_{ij}$ components using coordinate transformation rules.
(3) Lastly $\hat{Q}_{ij}$ is written in terms of $\hat{Q}_{kk}$ using the transformation rules.

In this scheme ε is assumed a function of C^2, where $C^2 = \frac{1}{3}(c_1^2 + c_2^2 + c_3^2)$, and is Taylor expanded about the steady state. After it is assumed that the perturbations are wavelike and axisymmetric, a seventh-order dispersion relation emerges of the same structure as (25) and dependent on the three parameters, ω_0, ω_0' and e, alongside k.

Given e, the marginal curves of the viscous instability and overstability are

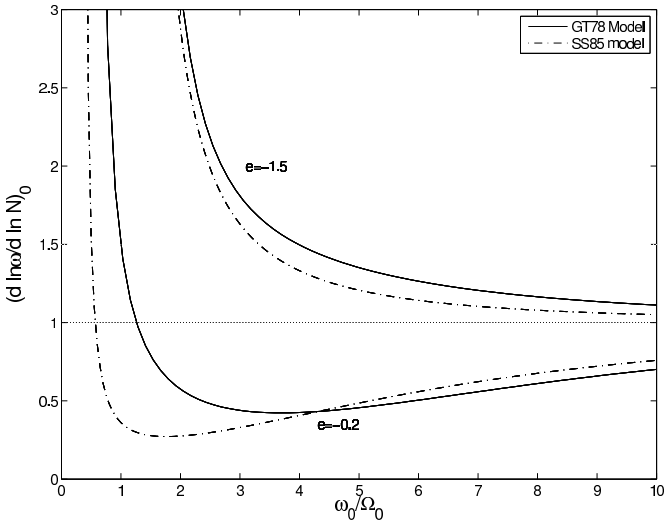

Fig. 8. Comparison between the SS85 and GT78 kinetic models with respect to the marginal curves of viscous instability, for $e = -0.2$ and $e = -1.5$. Regions above the curves are unstable

numerically determined in the (ω_0, ω_0') plane. They are plotted in Figs 8 and 9.

The curves for the viscous instability share the same qualitative features as those of the SS85 model. Though the former deviate somewhat in shape, their singularities approximately coincide, they asymptote to the line $\omega_0' = 1$, and the critical value of e (which determines whether a curve approaches this line from above or below) is roughly $-9/11$. This suggests that not only is the viscous mode resistant to the effects of non-locality in time (as proven in the previous section) but also to the details of the collision term, in particular to anisotropy, for which the Goldreich and Tremaine model accounts somewhat better.

Both branches of the curves of overstability agree in their general features with those of SS85. In the large ω_0 limit, the right branches asymptote to $\omega_0' = \text{cst}$; in the isothermal limit this constant is $2/9$, according with the SS85 and fluid models. However the critical e, below which marginal curves can cross into the first quadrant, is closer to -2.4 than -3. Also the left branches intersect the $\omega_0 = 0$ axis at slightly lower values: stability is assured in the region left of the singularity if $\omega_0' \lesssim 4.674$, as opposed to ≈ 5.192. We conclude that the linear stability of the viscous overstability is a little more sensitive to the details of the collision term, and hence anisotropy— though not nearly as much as to non-locality in time. As previously mentioned, the mechanism of overstability relies on the synchronisation of two oscillations, that of the acoustic-inertial wave, and that of a forcing which issues from the accompanying variation in angular momentum flux. The instability is vulnerable to disruption in the phase and in the magnitude of this forcing. A stress free to oscillate independently certainly impacts on the former. Anisotropy may

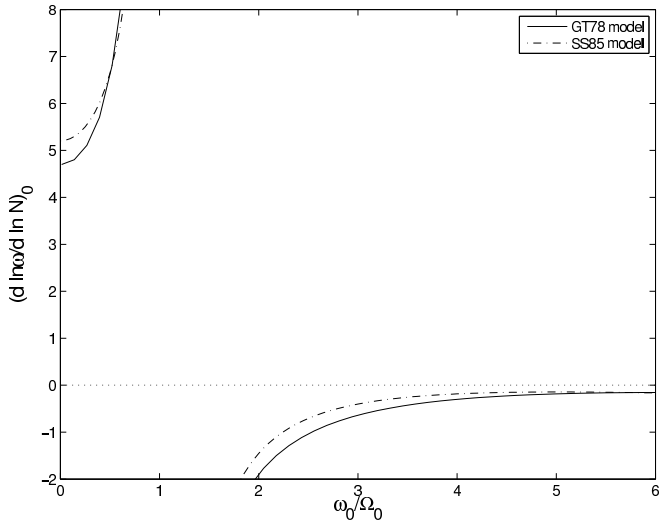

Fig. 9. Comparison between the SS85 and GT78 models with respect to the marginal curves of viscous overstability when $e = -0.2$. Regions above the left branch are unstable while regions below the right branch are unstable.

impact on the latter.

Lastly we resolve the potential 'anisotropic overstable' modes for low ω_0 and find them unstable for $e \lesssim -48$, far larger than predicted by the SS85 model (though still unfeasible). This emphasises again the fact that the two models differ most in their treatment of anisotropy. We conclude that the less accurate SS85 model, only linear in Π_{ij}, fails to fully model the deformations of the velocity ellipsoid.

6 Conclusion

In summary, we have calculated the linear stability of a patch of a dilute planetary ring in a shearing sheet employing a second-order kinetic theory. We have defined 'diluteness' as the insignificance of non-local effects, whose importance we can roughly quantify by $a\Omega/c$ for lower optical depths. But throughout Saturn's rings the velocity dispersion is low enough and particle size large enough, for this quantity to be non-negligible, thus we recognise that the applicability of a dilute model is restricted. Nevertheless this work reveals the interesting effects anisotropy and non-Newtonian stress have on the viscous instability and overstability. It also provides a preliminary framework in which a linear analysis of a dense gas may be undertaken.

We adopted a system of vertically integrated moment equations derived from Shu and Stewart's inelastic generalisation of the BGK equation in their 1985 paper. The ensuing system manifests both the viscous instability and over-

stability in the long-wavelength limit, and their extensions induced by self-gravity on intervals of intermediate wavelength. It predicts viscous or viscous/gravitational instability in dilute rings where particles collide about 3.5 times or more per orbit (optical thicknesses greater than 0.2, or less depending on the importance of self-gravity on the collision frequency). Viscous overstability does not feature in dilute regions.

These results were compared with a hydrodynamic model incorporating the kinetic theory's effective viscosity (evaluated at equilibrium) and cooling function. We find that the criterion for viscous instability is precisely the same as that for the kinetic model, but the two criteria diverge in the intermediate range of collision frequency for the viscous overstability. According to the kinetics, overstability is suppressed in this regime, a result in contradiction with the fluid model which predicts the instability to be widespread. We conclude that hydrodynamics presents a misleading impression of the viscous overstability's prevalence on small and intermediate ranges of ω_c/Ω_0, for a dilute ring. This arises from the increasingly non-Newtonian nature of the stress in this regime, an effect the kinetic account captures but which the hydrodynamical cannot. We stress that this incongruence will be most marked for a dilute ring; as the collisional stress tensor is local in time, we assume the denser the ring the better the hydrodynamic approximation.

We also undertook a linear stability analysis of the Goldreich and Tremaine 1978 kinetic model, employing a Boltzmann-type collision term with a triaxial Gaussian, which should factor in anisotropic effects more thoroughly. The criteria for viscous instability and overstability mirror qualitatively that of the SS85 model, and thus suggest that the linear dynamics of a disk are insensitive to the the precise details of the collision term. In particular, the criterion of viscous instability matches closely that of the SS85 model. The mechanism of this instability would thus seem relatively robust, not only resistant to the effects of non-locality in time but also of anisotropy. The discrepancy between the marginal curves of viscous overstability computed by the SS85 and GT78 models is a little more pronounced. We conclude the viscous overstability is relatively fragile for small and intermediate ω_c/Ω_0— very susceptible to non-locality in time and slightly altered by anisotropy

On intermediate and short scales the SS85 model also predicted the emergence of a quasi-thermal instability which the hydrodynamical analysis revealed to be associated with a mode orienting the thermal and density perturbations in such a way to keep the equation of motion undisturbed. This mechanism thus mimicks that operating in Field's thermal instability (Field 1965). We find that the instability should occur on optical thicknesses less than 2. However hydrodynamics shows that this instability is severely sensitive to heat conduction; κ need not be large to extinguish it entirely. Thus the omission of third-order moments in the kinetic model bestows on it a prominence that it does not de-

serve. When self-gravity is included intermediate scale instability can occur for much larger κ which in this case we refer to as a 'viscous/gravitational instability'. Self-gravity, in addition to its important dynamic role on intermediate scales, will enhance the collision frequency, and render the dependence of ω_c on N as steeply as $N^{3/2}$. In general this will make the system more susceptible to both the viscous instability and overstability on long lengthscales.

Two possibly fruitful avenues which proceed from this work are: linear stability calculations of dense and/or spinning particle disks, and nonlinear studies of the evolution of the viscous instability and overstability using the second-order moment equations.

In principle the techniques employed here can be set upon kinetic models of dense and spinning rings. Detailed formulations have been developed in Shukhman 1984, Araki and Tremaine 1986, Araki 1988 and Araki 1991, but, unmodified, their algebraical truculence surely prohibits all but equilibrium calculations. The success of the SS85 model encourages us that a simplification of the dense disk collision terms could provide a model that captures the essential physics, and also expedites linear and nonlinear analysis. The results obtained with such a model would be directly pertinent to N-body simulations and Saturn's B-ring. It could also ascertain the validity of the fluid description in the dense regime.

It would be instructive also to determine the impact of the nonlinear evolution of the second-order moments on the development of the instabilities discussed, as compared to the Newtonian fluid model, which so far has only been explored in the isothermal case (Schmit and Tscharnuter 1999). They may elicit interesting nonlinear behaviour from the viscous overstability. But an understanding of the small-scale instabilities, even if unphysical, is essential for the sucessful numerical implementation of these equations.

Acknowledgments

The manuscript was much improved thanks to the numerous and helpful comments of Juergen Schmidt. This research was funded in part by an award from the Leverhulme Trust. HNL acknowledges the financial support of the Cambridge Commonwealth Trust.

A Appendix: Dispersion Relation Coefficients

The coefficients appearing in the dispersion relation of the SS85 model (see Eq.(25)) are:

$$\mathsf{A} = \tfrac{2}{3}\omega_0 \frac{e(1+\omega_0^2) - 9(6+\omega_0^2)}{11+2\omega_0^2}, \tag{A.1}$$

$$\mathsf{B} = -4 - \frac{36}{11+2\omega_0^2}, \tag{A.2}$$

$$\mathsf{C} = \frac{2\,e\,\omega_0^2(1+\omega_0^2) - (55+52\omega_0^2+6\omega_0^4)}{11+2\omega_0^2}, \tag{A.3}$$

$$\mathsf{D} = \frac{2\omega_0}{9(11+2\omega_0^2)^2}\Big[20e(10+11\omega_0^2+\omega_0^4) + 3\omega_0'(198+36\omega_0^2) - 3(4084+1037\omega_0^2+58\omega_0^4)\Big], \tag{A.4}$$

$$\mathsf{E} = \frac{\omega_0}{3(11+2\omega_0^2)}\Big[e(13+19\omega_0^2+6\omega_0^4) - 3(80+31\omega_0^2+2\omega_0^4)\Big], \tag{A.5}$$

$$\mathsf{F} = -\frac{12(10+\omega_0^2)^2}{(11+2\omega_0^2)^2}, \tag{A.6}$$

$$\mathsf{G} = \frac{2}{9(11+2\omega_0^2)}\Big[e\,\omega_0^2\,(553+599\omega_0^2+46\omega_0^4) - 27\,e\,\omega_0'\,\omega_0^2(1+\omega_0^2) + \omega_0'\,\omega_0^2\,(2349+405\omega_0^2) + (-3960-13785\omega_0^2-2856\omega_0^4-132\omega_0^6)\Big], \tag{A.7}$$

$$\mathsf{H} = \frac{1+\omega_0^2}{3(11+2\omega_0^2)}\Big[e\,\omega_0^2(17+2\omega_0^2) - (132+18\omega_0^2)\Big], \tag{A.8}$$

$$\mathsf{I} = \frac{4\omega_0}{9(11+2\omega_0^2)^3}\Big[2e\,(700+849\omega_0^2+156\omega_0^4+7\omega_0^6) \\ +3\omega_0'\,(1980+558\omega_0^2+36\omega_0^4)-3(21460+7344\omega_0^2+789\omega_0^4+28\omega_0^6)\Big]\,, \tag{A.9}$$

$$\mathsf{J} = \frac{2\omega_0}{9(11+2\omega_0^2)^2}\Big[e\,(1+\omega_0^2)(80+32\omega_0^4+\omega_0^2(478-99\omega_0'))) \\ -3(10\omega_0^6+\omega_0^2(1977-819\omega_0')+\omega_0^4(303-135\omega_0')+4(250+99\omega_0'))\Big]\,, \tag{A.10}$$

$$\mathsf{K} = \frac{\omega_0}{3(11+2\omega_0^2)}\Big[e\,(11+17\omega_0^2+6\omega_0^4)-3(44+25\omega_0^2+2\omega_0^4)\Big]\,, \tag{A.11}$$

$$\mathsf{L} = \frac{4\omega_0^2}{9(11+2\omega_0)^3}\Big[e\,(1+\omega_0^2)(2240+20\omega_0^4+\omega_0^2(451-36\omega_0')-270\omega_0') \\ -6(5156+5\omega_0^6+\omega_0^2(1578-459\omega_0')-2034\omega_0'-9\omega_0^4(-17+2\omega_0'))\Big]\,, \tag{A.12}$$

$$\mathsf{M} = \frac{2\omega_0^2}{3(11+2\omega_0^2)^2}\Big[e\,(1+\omega_0^2)(25+2\omega_0^4+\omega_0^2(45-30\omega_0')+33\omega_0') \\ +6(\omega_0^4(-4+6\omega_0')-2(8+33\omega_0')+\omega_0^2(-47+48\omega_0'))\Big]\,, \tag{A.13}$$

$$\mathsf{N} = \frac{1}{3}\,e\,\omega_0^2(1+\omega_0^2), \tag{A.14}$$

$$\mathsf{P} = \frac{4\omega_0^3}{3(11+2\omega_0^2)^3}\Big[e\,(1+\omega_0^2)(176+2\omega_0^4+\omega_0^2(43-12\omega_0')-114\omega_0') \\ +72\omega_0'(25+4\omega_0^2)\Big]\,, \tag{A.15}$$

$$\mathsf{Q} = -\frac{2\omega_0^3}{(11+2\omega_0)^2)}\Big[e\,(1+\omega_0^2)\{2\omega_0^2(-1+\omega_0')-11(1+\omega_0')\}-18\omega_0'\,\omega_0^2\Big]\,, \tag{A.16}$$

$$\mathsf{R} = -\frac{4\omega_0}{3(11+2\omega_0^2)}\Big[e\,(1+\omega_0^2)-9(6+\omega_0^2)\Big]\,, \tag{A.17}$$

$$\mathsf{S} = 2+\frac{18}{11+2\omega_0^2}, \tag{A.18}$$

$$\mathsf{T} = -\frac{4(1+\omega_0^2)}{11+2\omega_0^2}\Big[e\,\omega_0^2-22-3\omega_0^2\Big]\,, \tag{A.19}$$

$$\mathsf{U} = \frac{4\omega_0}{3(11+2\omega_0^2)^2}\Big[-2e\,(10+11\omega_0^2+\omega_0^4)+3(316+77\omega_0^2+4\omega_0^4)\Big]\,, \tag{A.20}$$

$$\mathsf{V} = -\frac{2\omega_0}{3(11+2\omega_0^2}\Big[e\,(11+17\omega_0^2+6\omega_0^4)-3(44+25\omega_0^2+2\omega_0^4)\Big]\,, \tag{A.21}$$

$$\mathsf{W} = -\frac{4\omega_0^2}{3(11+2\omega_0^2)^2}\left[e\,(49+53\omega_0^2+4\omega_0^4)-6(133+26\omega_0^2+\omega_0^4)\right], \quad \text{(A.22)}$$

$$\mathsf{X} = -\tfrac{2}{3}\,e\,\omega_0^2(1+\omega_0^2), \quad \text{(A.23)}$$

$$\mathsf{Y} = -\frac{4\omega_0^3}{3(11+2\omega_0^2)^2}\left[e(29+31\omega_0^2+2\omega_0^4)-18(10+\omega_0^2)\right]. \quad \text{(A.24)}$$

B Appendix: Critical Self Gravity Constant

We present the expression for the critical value of g above which gravitational/viscous instability arises in the SS85 kinetic model. See Section 3.1.1.

$$g_{\rm crit} = 8\,\frac{\omega_0^3\,[h_1(\omega_0,e)+h_2(\omega_0,e)\,\omega_0'+h_3(\omega_0,e)\,\omega_0'^2]}{(11+2\omega_0^2)^3(e(29+31\omega_0^2+2\omega_0^4)-18(10+\omega_0^2))} \quad \text{(B.1)}$$

where

$$h_1 = -e^2(16+\omega_0^2)(11+13\omega_0^2+2\omega_0^4)^2,$$
$$h_2 = e(11+13\omega_0^2+2\omega_0^4)\left[e(-62-29\omega_0^2+35\omega_0^4+2\omega_0^6)-18(100+32\omega_0^2+\omega_0^4)\right],$$
$$h_3 = -6\left[216\omega_0^2(25+4\omega_0^2)-6e(-550-481\omega_0^2+91\omega_0^4+22\omega_0^6)\right.$$
$$\left.+e^2(1+\omega_0^2)^2(-209+16\omega_0^2+4\omega_0^4)\right]$$

C Appendix: Critical Coefficient of Heat Diffusivity

Here we list the critical κ below which quasi-thermal instability occurs on a band of wavelengths for a viscous fluid model without self-gravity.

$$\kappa_{\rm crit} = \frac{9(1+\xi)^2\nu_0^2+(1+\xi)\nu_0(4\Gamma_{\rm N}+4\Gamma_{\rm T}-9\nu_{\rm T})-8\Gamma_{\rm N}\nu_{\rm T}}{12(1+\xi)^2\nu_0}$$
$$-4\frac{\sqrt{(4\Gamma_{\rm N}+9(\xi+1)\nu_0)((\xi+1)\nu_0-\nu_{\rm T})((\xi+1)\Gamma_{\rm T}\nu_0-\Gamma_{\rm N}\nu_{\rm T})}}{12(1+\xi)^2\nu_0} \quad \text{(C.1)}$$

When self-gravity is present, the marginal curves in the (ω_0,ω_0') plane for given k, κ and e may be determined from Eq.(41) with heat flux terms added. For

a dilute ring with an equilibrium computed by SS85, we obtain

$$\omega_c' = -\frac{11+2\omega_0^2}{3\left[18\omega_0^3+33\omega_0 k^2+\omega_0 e(11+9\omega_0^2-2\omega_0^4)+\kappa k^2(4\omega_0^4-121)\right]} \times \left[\omega_0(1+\omega_0^2)(3+k^3)\,e+2gk\omega_0(9-e(1+\omega_0^2))-\kappa k^2(11+2\omega_0^2)(3-2gk+k^2)\right]. \tag{C.2}$$

References

[1] Araki, S., 1988: 'The Dynamics of Particle Disks, II. Effects of Spin Degrees of Freedom', *Icarus*, **76**, 182-198.

[2] Araki, S., 1991. The Dynamics of Particle Disks III, Dense and Spinning Particle Disks. *Icarus*, **90**, 139-171.

[3] Araki, S., Tremaine, S., 1986. The Dynamics of Dense Particle Disks. *Icarus*, **65**, 83-109.

[4] Binney, J., Tremaine, S., 1987. *Galactic Dynamics*. Princeton University Press. Oxford University, England.

[5] Bhatnagar, P.L., Gross, E.P., Krook, M., 1954. A model for collisional processes in gases. I. Small amplitude processes in charged and neutral one-component systems. *Physical Review*, **94**, 511-525.

[6] Bridges, F., Hatzes A., Lin, D.N.C., 1984. Structure, Stability and Evolution of Saturn's Rings. *Nature*, **309**, 333-335.

[7] Chapman, S., Cowling, T.G., 1970. *The Mathematical Theory of Nonuniform Gases*, 3rd ed. Cambidge University Press, Cambridge, UK.

[8] Cuzzi, J.N., Lissauer, J.J., Esposito, L.W., Holberg, J.B., Marouf, E.A., Tyler, G.L., Boischot, A., 1984. Saturn's Rings: Properties and Processes. In: In Greenberg, R., Brahic, A. (Eds.). *Planetary Rings*. University of Arizona Press, Tucson, Arizona.

[9] Cuzzi, J.N., Estrada, P.R., 1996. Voyager Observations of the Color of Saturn's Rings. *Icarus*, **122**, 251-272.

[10] Dilley, J.P., 1993. Energy Loss in Collisions of Icy Spheres: Loss Mechanism and Size-Mass Dependence. *Icarus*, **105**, 225-234.

[11] Dilley, J., Crawford, D., 1996. Mass dependence of energy loss in collisions of icy spheres: An experimental study. *Journal of Geophysical Research*, **101**, 9267-9270.

[12] Durisen, R.H., 1995. An instability in planetary rings due to ballistic transport. *Icarus*, **115**, 66-85.

[13] Field, G.B., 1965. Thermal Instability. *Astrophysical Journal*, **142**, 531-567.

[14] Goertz, C.K., Morfill, G., 1988. A new instability of Saturn's rings. *Icarus*, **74**, 325-330.

[15] Goldreich, P., Tremaine, S., 1978. The Velocity Dispersion in Saturn's Rings. *Icarus*, **34**, 227-239.

[16] Goldreich, P., Tremaine, S., 1982. The Dynamics of Planetary Rings. *Annual Review of Astronomy and Astrophysics*, **20**, 249-283.

[17] Hämeen-Anttila, K.A., 1978. An Improved and Generalised Theory for the

Collisional Evolution of Keplerian Systems. *Astrophysical Space Science*, **58**, 477-519.

[18] Hatzes, A.P., Bridges, F.G., Lin, D.N.C., 1988. Collisional properties of ice spheres at low impact velocities. *Monthly Notices of the Royal Astronomical Society*, **231**, 1091-1115.

[19] Hatzes, A.P., Bridges, F., Lin, D.N.C., Sachtjen, S., 1991. Coagulation of Particles in Saturn's Rings: Measurements of the Cohesive Force of Water Frost. *Icarus*, **1991**, 113-121.

[20] Horn, L.J., Cuzzi, J.N., 1995. Characteristic Wavelengths of Irregular Structure in Saturn's B Ring. *Icarus*, **119**, 285-310.

[21] Julian, W.H., Toomre, A., 1966. Non-Axisymmetric Responses of Differentially Rotating Disks of Stars. *Astrophysical Journal*, **146**, 810.

[22] Kato, S., 1978. Pulsational instability of accretion disks to axially symmetric oscillations. *Monthly Notices of the Royal Astronomical Society*, **185**, 629-642.

[23] Lin, D.N.C., Bodenheimer, P., 1981. On the Stability of Saturn's Rings. *The Astrophysical Journal*, **248**, L83-L86.

[24] Lukkari, J., 1981. Collisional Amplification of Density Fluctuations in Saturn's rings. *Nature*, **292**, 433-435.

[25] Lukkari, J., 1989. Velocity dispersion in particulate disks with size distribution. *Earth, Moon, Planets*, **44**, 207-218.

[26] Marouf, E.A., Tyler, G.L., Zebker, H.A., Simpson, R.A., Eshleman, V.R., 1983. Particles Size Distributions in Saturn's Rings from Voyager 1 Radio Occultation. *Icarus*, **54**, 189-211.

[27] McDonald, J.S.B., Hatzes, A., Bridges, F., Lin, D.N.C., 1989. Mass Transfer during Ice Particle Collisions in Planetary Rings. *Icarus*, **82**, 162-179.

[28] Morishima, R., Salo, H., 2006. Simulations of dense planetary rings IV. Spinning self-gravitating particles with size distribution. *Icarus*, **181**, 272-291.

[29] Porco, C.C. and 34 colleagues, 2005. Cassini Imaging Science: Initial Results on Saturn's Rings and Small Satellites. *Science*, **307**, 1226-1236

[30] Salo, H., 1987. Collisional evolution of rotating, non-identical particles. *Earth, Moon, and Planets*, **38**, 149-181.

[31] Salo, H., 1991. Numerical Simulations of Dense Collisional Systems. *Icarus*, **90**, 254-270.

[32] Salo, H., 1992a. Gravitational wakes in Saturn's rings. *Nature*, **359**, 619-621.

[33] Salo, H., 1992b. Numerical simulations of dense collisional systems II. Extended distribution of particle sizes. *Icarus*, **96**, 85-106.

[34] Salo, H., 2001. Numerical Simulations of the Collisional Dynamics of Planetary Rings. In: Pöschel, T., Luding, S., (eds.). Granular Gases. *Lecture Notes in Physics*, **564**, 330.

[35] Salo, H., Schmidt, J., Spahn, F., 2001. Viscous Overstability in Saturn's B Ring: I. Direct Simulations and Measurement of Transport Coefficients. *Icarus*, **153**, 295-315.

[36] Schmidt, J., Salo, H., 2003. Weakly Nonlinear Model for Oscillatory Instability in Saturn's Dense Rings. *Physical Review Letters*, **90**, 61102.

[37] Schmidt, J., Salo, H., Spahn, F., Petzschmann, O., 2001. Viscous Overstability in Saturn's B-Ring, II. Hydrodynamic Theory and Comparison to Simulations. *Icarus*, **153**, 316-331.

[38] Schmit, U., Tscharnuter, W.M., 1995. A Fluid Dynamical Treatment of the Common Action of Self Gravitaton, Collisions and Rotation in Saturn's B-Ring. *Icarus*, **115**, 304-319.

[39] Schmit, U., Tscharnuter, W.M., 1999. On the Formation of the Fine-Scale Structure in Saturn's B Ring. *Icarus* **138**, 173-187.

[40] Shu, F.H., Stewart, G.R., 1985. The Collisional Dynamics of Particulate Disks. *Icarus* **62**, 360-383.

[41] Shu, F.H., Dones, L., Lissauer, J.L., Yuan, C., Cuzzi, J.N., 1985. Nonlinear Spiral Density Waves: Viscous Damping. *The Astrophysical Journal*, **299**, 542-573.

[42] Shukhman, I.G., 1984. Collisional dynamics of particles in Saturn's rings. *Soviet Astronomy*, **28**, 574-584.

[43] Spahn, F., Schmidt, J., Petzschmann, O., 2000: 'Stability Analysis of a Keplerian Disk of Granular Grains: Influence of Thermal Diffusion'. *Icarus*, **145**, 657-660.

[44] Stewart, G.R., Lin, D.N.C., Bodenheimer, P., 1984. Collisional Transport Processes. In: Greenberg, R., Brahic, A., (eds.). *Planetary Rings*. University of Arizona Press, Tucson, Arizona.

[45] Supulver, K.D., Bridges, F.G., Lin, D.N.C., 1995. The Coefficient of Restitution of Ice Particles in Glancing Collisions: Experimental Results for Unfrosted Surfaces. *Icarus*, **113**, 188-199.

[46] Supulver, K.D., Bridges, F.G., Tiscareno, S., Lievore, J., Lin, D.N.C., 1997. The Sticking Properties of Water Frost Produced under Various Ambient Conditions. *Icarus*, **129**, 539-554.

[47] Thiessenhusen, K., Esposito, L.W., Kurths, J., Spahn, F., 1995. Detection of hidden resonances in Saturn's B-ring. *Icarus*, **113**, 206-212.

[48] Toomre, A., 1964. On the gravitational stability of a disk of stars. *Astrophysical Journal*, **139**, 1217-1238.

[49] Tremaine, S., 2003. On the Origin of Irregular Structure in Saturn's Rings. *The Astronomical Journal*, **125**, 894-901.

[50] Ward, W.R., 1981. On the Radial Structure of Saturn's Rings. *Geophysical Research Letters*, **8,6**, 641-643.

[51] Wisdom, J, Tremaine, S., 1988. Local Simulations of Planetary Rings. *The Astronomical Journal*, **95**, 925-940.

[52] Zebker, H.A., Marouf, E.A., Tyler, G.L., 1985. Saturn's Rings: Particle Size Distributions for Thin Layer Models. *Icarus*, **64**, 531-548.